Additive Manufacturing of Functionally-Graded Porous Biodegradable Scaffolds using Sacrificial Porogens

by

Farid Behzadian

A thesis
presented to the University of Waterloo
in fulfillment of the
thesis requirement for the degree of
Master of Applied Science
in
Mechanical Engineering

Waterloo, Ontario, Canada, 2015

AUTHOR'S DECLARATION

I hereby declare that I am the sole author of this thesis. This is a true copy of the thesis, including any required final revisions, as accepted by my examiners.

I understand that my thesis may be made electronically available to the public.

Abstract

The focus of this dissertation is on the additive manufacturing (AM) of a porous biodegradable scaffold using a fine Calcium Polyphosphate (CPP) powder, with the aid of sacrificial porogens. CPP is a member of Calcium Phosphate (CaP) bioceramic family which has shown great potential in bone tissue engineering over the past years. AM processes are fairly new technologies that have been involve in many different industries and applications, including bone tissue engineering. Not too long ago, CPP was investigated using a powder based 3D printing technique, which is an AM process, and it was revealed that this new manufacturing process offers a great potential in improving previous finding made by traditional fabrication techniques. Over the past few years there have been many different studies on 3D printing CPP substrate, but almost all of those studies were based on using a large particle CPP powder.

In this study, the fabrication of CPP structures was based on using a fine CPP powder with a particle size of < 75μm. 3D printing fine dry powder has one main challenge which is flowability of the powder, and in this study a new solution has been suggested to improve the flow behavior of the fine CPP powder. Polyvinyl Alcohol (PVA) powder with a particle size of 75-106 μm was chosen as the large sacrificial particles so called porogens, to be mixed with fine CPP powder to improve the flowability. In order to improve the flow behavior of the powder in the AM process, various percentages of porogens were mixed with the fine CPP powder to fine the appropriate dosage. Furthermore, there were two different liquid binders tested in the AM process. After CPP parts were fabricated, all specimens were measured in dimensions before and after the sintering. The dimensional measurements were

used to determine the shrinkage percentage. Then the sintered parts had to be tested one by one through Archimedes method to find the porosity percentage corresponding to each individual sample. Following that, uniaxial compression test was applied to evaluate the mechanical strength of each specimen. In order to look at the micro structures of samples and making sure the particle have formed good bonding/sinter necks, random specimens were chosen to me examined using Scanning Electron Microscopy (SEM). Moreover, different powders were sent to an external facility to be tested for the flow behavior and the average particle size by using a rheometer and a laser diffraction method, respectively.

The results were analyzed for different categories based on the pre mixed porogens percentage. It was proven that adding porogens definitely improves the flowability of the fine powder; it also increases the shrinkage percentage of samples. Then the results were compared with previous findings that were based on using a large particle CPP powder; it was shown that some of those previous finding obtain by 3D printing large particle CPP powder, can be achieved by doing the same using the fine CPP powder. Furthermore, a new higher compressive strength was reported in this study that was not achieved in previous reports which was based on the large particle CPP powder.

Acknowledgements

I would like to take this opportunity to thank the people who helped me along this academic journey.

I was blessed and very lucky to have Prof. Ehsan Toyserkani as my supervisor and I will always be truly grateful for his encouragement, guidance and constant support throughout this academic journey. I learned many lessons under his mentorship which I will always keep by my side in my life and career ahead. I would also like to show my gratitude to Dr. Mihaela Vlasea for her enthusiastic visions for this project, kind support, and being the most helpful person in this academic experience after Prof. Ehsan Toyserkani.

I hereby acknowledge my thesis examining committee members, Dr. Shahrzad Esmaeili and Dr. Soo Jeon from the University of Waterloo for taking their valuable time to review my thesis and to provide their valued comments.

I would also like to thank Eugene Hu in the Institute of Biomaterials and Biomedical Engineering at the University of Toronto for his advices; without him sintering my samples and his hard work in providing me with raw materials in my project, this thesis would not have been possible.

I would like to extend a special thanks to Joseph Emili at ATS Scientific Inc. for helping me characterizing some of my powder materials in their labs using their equipment. I also like to express my appreciation to CNC technician Robert Wagner at the University of Waterloo for helping me fabricating number of modification compartments.

I would like to show my gratitude to my friends and colleagues in the Multi Scale Additive Manufacturing Laboratory at the University of Waterloo, Amir Azhari, Ahmad Basalah, Richard Liang, Esmat Sheydaeian, and Elahe Jabari for their assistance and friendship.

I owe my highest gratitude to my beloved parents, Maryam and Reza, who sacrificed themselves and everything they had to raise me, and were always supportive of my choices in life. Thanks to my brothers, Farshad and Farhad, for being there for me whenever I needed them. I also like to take a moment and show my gratitude to my grandfather, Mehdi Behzadi, bless his soul, who always had faith in me and encouraged me to pursue my education.

Dedication

I dedicate this work to my father, my role model and the greatest inspiration I ever had ; if it wasn’t for him I would not have made it this far.

Table of Contents

List of Figures

List of Tables

Chapter 1
Introduction

1.1 3D Printing in Tissue Engineering

Bone injuries and related diseases are common in today's society and every year there are more than 2 million bone graft procedures happening around the globe [1]. For the past 30 years, significant amount of research has been done toward bone grafting to investigate suitable synthetic porous materials to replace the missing bone in human's body [2]. However, only 10 percent of those 2 million procedures mentioned earlier used synthetic materials as bone grafts and in the rest of those operations natural bone from autografts or allografts were being used [1]. Synthetic bone scaffolds are becoming more on demand and crucial; and there are two reasons for that. The first reason is that autografts have limited availability; the second reason is every time allografts are being used there is a risk of disease transfer [3]. In the year 2000, Hutmacher et al stated that a synthetic scaffold should have 4 main characteristics including [4]:

- It should have a suitable surface chemistry for cell attachment, proliferation, and differentiation
- It should be three-dimensional and highly porous with an interconnected pore network for cell growth and flow transport of nutrients and metabolic waste
- It should have acceptable mechanical properties to match those of the tissues at the site of implantation

- It should be biocompatible and bioresorbable with a controllable degradation and resorption rate to match cell/tissue growth in vitro and/or in vivo.

Through the past decade, different studies have shown that calcium polyphosphate (CPP), a member of calcium phosphate family has significant potential to be a worthy bone substitute substrate candidate for bone and cartilage tissue engineering applications [5–8].

The traditional way of creating anatomically shaped CPP was to use computer numerical control (CNC) machining which is a subtractive method used to mill a large sintered block of CPP to its final desirable shape. This method is time consuming and has substantial amount of CPP material waste, which leads to increase the fabrication cost [9]. Moreover, it is difficult to machine this type of porous ceramic due to cracking and fracture defects [10].

However over the past 9 years, a research team at the Multi Scale Additive Manufacturing (MSAM) lab in University of Waterloo started to work on manufacturing CPP implants using 3D printing [11]. This became possible by collaboration with another research team at University of Toronto which was involved in refining the composition and thermal processing of CPP for making it appropriate for bone substituting [12–14].

Controlling porosity could be challenging and difficult when it comes to design and create a scaffold with a complex shape/architecture using commonly used scaffold processing techniques. Particulate leaching, gravity casting, freeze drying, foaming agents, porogens, and hot pressing are some of those common conventional methods used for the fabrication of functionally graded porous structures [4, 15, 16]. The main challenge with

these conventional methods is the poor consistency, which is due to the high sensitivity to variants in process parameters [15]. However, since the introduction of additive manufacturing (AM) techniques, most of these difficulties have been addressed and solved accordingly. AM techniques, including selective laser sintering (SLS), Fused Deposition Modeling (FDM), and 3D Printing have shown promising results in different areas in tissue engineering and started to merge with the bio-medical industry in various fields.

3D printing is a powder-based AM technique that has become very popular in tissue engineering to generate polymer[17], metallic [18], and bioceramic parts [6, 19]. 3D printing is more often preferred to other AM techniques like SLS and FDM, and probably it is the most widely investigated technique when it comes to fabricating bone substitute scaffolds[16]. This can be attributed to the simplicity of the process and absence of using laser which makes it more users friendly and more cost effective. Furthermore this process is compatible with diverse range of powder materials including ceramics, metals, and polymers. 3D printing is capable of creating a complex shape scaffold that has specific exterior and interior architecture with control over the porosity.

1.2 Advancements in powder-based additive manufacturing via 3D Printing

The current study is based on the previous work and on-going investigation at Multi Scale Additive Manufacturing (MSAM) lab at University of Waterloo and the collaboration with a research team at the University of Toronto [6, 11, 20, 21]. During the past decade, there has been a large number of studies about Calcium polyphosphate (CPP), showing its potential as a bone substituting substrate [5–8, 13, 14, 22]. The research team at MSAM lab

has been working on manufacturing CPP implants using a powder based 3D printing system; MSAM group has been working on characterizing the manufacturing process and investigating the related limitations/boundaries.

3D printing CPP powder with particle size 75-150µm was done by Shanjani et al. using a conventional 3D printer (Zprinter® 310plus, Z Corporation, Burlington, MA, US) [6, 11, 20]. An average volume present porosity of 38±1% was achieved using the Archimedes method with a pore size range of (~5-258 µm)[9]; The reported compressive mechanical strength of 3D printed CPP structures was ~ 50 MPa which is about 150% higher than measured strength of the conventional sintered parts[9, 23]. Following Shanjani et al. 's work, a new multi scale AM system was developed in MSAM lab at university of waterloo [15, 19, 21, 24]; Vlasea et al. used this new multi scale AM system to 3D print CPP structures using two different particle sizes including (CPP 75-150 µm) and (CPP < 75µm) [15]. The 3D printed CPP parts by Vlasea et al. had a porosity range between 30-55% with a range of compressive strength between 2.9-45.1 MPa [15].

Almost all of the previous CPP related additive manufacturing studies were based on using large particle CPP powder (75-150 µm) [6, 9, 15, 20, 23]. One of the main challenges with the fine powder is the flowability, and according to previous studies larger particles with a spherical shape intend to have better flowability [3, 25, 26]; however, smaller particle size in a powder could lead to increase the packing density which can improve the sintering and mechanical properties [3, 25].

In this study, a solution was suggested to improve the flow behavior of a fine powder which in this case means CPP powder with a particle size < 75 µm. 3D printing fine CPP powder was performed successfully and the new findings were reported.

1.3 Objectives of the Thesis

The present thesis is an initial step to develop information for investigating the effect of using smaller CPP powder size in conjunction with porogens material to improve mechanical and structural properties of bone substitutes.

To achieve this goal, the following tasks were carried out:

- **Production:** 3D printing porous CPP scaffolds using fine powder (CPP < 75 µm),
    - Choosing the proper porogens particle size.
    - Choosing the appropriate porogens percentage.
- **Characterization:** Evaluating the engineering properties of 3D printed CPP implants
    - Powder characterization (particle size, flowability)
    - Porosity investigation
    - Characterization of mechanical strength in compression
    - Structural characterization (SEM)
    - Statistical evaluations

1.4 Summary of content

The present thesis includes five chapters. Chapter 1 provides a general overview of motivation and limitation behind this study as well as the objectives of this thesis. In Chapter 2, a general view of biodegradable implants and their importance is first introduced, and then the background information on CPP is explained. Furthermore, Chapter 2 outlines the literature review on additive manufacturing, more specifically 3D printing and its principles. Chapter 3 describes in details the methodology behind each step of the way including material preparation, manufacturing process, post processing, and characterization techniques. Chapter 4 covers all data and result analysis gathered from all of the experiments and it includes all discussions related to each individual experiment and the relationship to others. At last, Chapter 5 addresses what was achieved through this study as a conclusion and what it leads to as suggested future work.

Chapter 2
Literature Review

2.1 Biodegradable Implants

In the biomedical industry when it comes to implantation, an important focus is on the properties of the constitutive material. Orthopedic implants are commonly divided into two groups: metallic implants and nonmetallic implants.

Metallic implants are more traditional and common to use due to their high strength and durability. Ttitanium based implants are the most popular metallic implants in orthopedics. Most of nonmetallic implants are made from materials that are fully or partially biodegradable, which means these types of implants will get integrated into the body implanted, in certain amount of time. Because of biodegradability, nonmetallic implants have gained more attention than before compare to metallic implants [27].

Nowadays, there is a considerable need for bone implants and synthetic bone substitutes due to a large number of bone injuries in the world. Biodegradability of non-metallic materials is a vital property for bone implants and synthetic bone substrates. The contrary to metallic implants, biodegradable implants do not need to be removed after surgery. Furthermore, after implanting a biodegradable structure, the initial stability of the fixation is preserved, and depending on the integration rate and the loss of strength during degradation in the surrounding environment, the stresses are transferred from the implant to the healing bone, which will promote faster healing and better long term stabilization [28, 29]. Also, avoiding the second operation will lead to a financial advantage for the patient and reduces the cost for the operative treatment of injuries [28].

2.1.1 Bioceramics

Bioceramics and biopolymers are the two main material groups in nonmetallic that have the most capable candidates for bone implants and synthetic bone substrates [30–32]. Nowadays, bioceramics are being used in many different applications including structural functions as joints, tissue replacements, and coating on metallic implants to promote better biocompatibility [33, 34].

Table 1. Bioceramics categorization based on reactivity [33]

Category	Inert Ceramics	Degradable/Resorbable Ceramics	Surface active ceramics (semi-inert)
Description	Don't show any sign of decay, wear, or react to the host environment	Digested and replaced by the presence of a biological environment	React to the host or physiological environment causing surface chemical change
Application	Total hip replacement prostheses, dental Crowns, bone plates, bone screws	Focal defect repair	Surface coating of metallic implants promoting strong bond
Materials	Alumina, Zirconia, glass	Tricalcium phosphate, Hydroxyapatite	Fully dense glass ceramic and hydroxyapatite

There are different ways to categorize ceramics; these categorizations are usually based on their reactivity, composition, or general form. However in the biomedical area of research, ceramics are commonly being categorized based on their reactivity as inert ceramics,

degradable or resorbable ceramics, and surface active ceramics [33]. Table 1 shows the description for each category and example of their applications.

The bone tissue matrix is very complex; however, structurally, it is composed of two types of zones; cortical and trabecular. Cortical bone is very dense; in addition this type of bone segment is found the near surface and exterior of a typical bone in the human body. Trabecular bone, also known as cancellous or spongiosa, is highly porous. Table 2 lists the range of compressive strengths and young modulus for both bone tissue types. The mineralized portion of the cortical bone is mostly made of calcium and phosphate ions [34, 35].

Table 2. Compressive strengths and young's modules for cortical and trabecular bone types [36]

	Cortical bone	**Trabecular bone**
Compressive strength (MPa)	100-230	2-12
Young’s modulus (GPa)	7-30	0.005-0.5

Between all bioceramics, calcium phosphate (CaP) ceramics have become more popular than the others due to their high biocompatibility and other qualities such as biodegradability and their osteoconductive capabilities [37–40]. Porous hydroxyapatite and tricalcium phosphate are the two popular member of calcium phosphate (CaP) ceramics that have shown successful results in in-vitro, in-vivo, and clinical studies [41–44].

2.1.1.1 Calcium Polyphosphate

Calcium polyphosphate (CPP) is another family member of calcium phosphate (CaP) ceramics and it has a Ca/P ratio of 0.5 [14]; "*this ratio allows CPP molecules to have similar chain-like configuration as a polymer molecules. At this configuration the oxygen-bridged links can form polyphosphates (linear structures), metaphosphates (ring structures), or ultraphosphates (cage structures) in an organized distribution in a crystalline state or with a random distribution in an amorphous state*" [45]. Recently this member of condensed phosphate family has become the point of interest in different bone related applications [46]. Studies have proven that CPP is osteoconductive and osteoinductive [7, 20, 47].

According to Pilliar et al., in order to make CPP powder the first step is calcining of the precursor powder, calcium phosphate monobasic monohydrate; in other words certain amount of $Ca(H_2PO_4)_2{\cdot}H_2O$ is placed in a platinum crucible and calcined at 500^{o}C for 10 hours in an air furnace to create CPP through the following chemical reaction [13]:

$$n\,Ca(H_2PO_4)_2\ .\ H_2O \xrightarrow{500^{o}C} [Ca(PO_3)_2]_n + 3n\,H_2O \qquad (1)$$

The resulting powder is then heated to 1100^{o}C which gets melted due to atmospheric conditions; this produces an amorphous glass and held under the same temperature for 1 hour to induce chain lengthening[13, 14]. Next, in order to form an amorphous frit, the molten CPP is quenched in distilled water to be cooled rapidly. Then by using 100% ethanol the frit gets dried to get rid of absorbed water and kept in a vacuum desiccator. The generated amorphous frit gets milled by stainless steel mortar and balls to produce CPP powder in different particle sizes, followed by screening[13, 14].

In the past two decades, there has been significant number of research including in-vitro and in-vivo studies around calcium polyphosphate providing strong evidences showing that CPP could be a good candidate with lots of potential for biodegradable synthetic bone substitute applications [5, 7, 8, 13, 14, 48–50]. Recent studies on CPP carried out by Pilliar and his research group have provided evidence of bone in-growth in both in vitro and in vivo studies [8, 13, 50, 51]. At first almost all of the focus was dedicated towards demonstrating that CPP is biocompatible as well as investigating the necessary requirements of CPP to be used as a synthetic bone substrate. Once the biocompatibility potential of CPP was proven, research groups started to look at methodologies for shaping CPP into a desirable 3D geometry. Initially, gravity sintering was used to fabricate CPP porous structures [8, 13]. In 2001, Porter et al started investigating a Solid Free-form Fabrication (SFF) technique, to be more specific it was a Stereolithography (SLA)-based technology [14]. During this study, SFF was used to fabricate porous CPP parts and processing parameters for this fabrication method was examined and recognized. Few years later, Wei et al. followed by Shanjani et al. started studying a powder based three dimensional printing (3D Printing) technology to fabricate porous CPP sample [6, 9, 11, 46].

2.2 Additive Manufacturing

Additive manufacturing was formerly known as rapid prototyping or sold free form fabrication. In the past, this technique was only used to manufacture only prototypes for 3D-modelling of the structures. However, the functionality of the technique has changed since real and applicable 3D-structures are manufactured using this technique. Due to this evolution American Society for Testing and Materials (ASTM) International has replaced the

old term “Rapid Prototyping” (RP) with a new term called “Additive Manufacturing” (AM) [26].

The traditional subtractive manufacturing techniques involve a careful and comprehensive analysis of the part’s geometry which will be used to find what tools and processes must be chosen to generate each particular feature within the design [26]. Furthermore, this geometry analysis determines the fabrication order of all features within the part design and shows if additional fixtures may be needed to manufacture the part When it comes to additive manufacturing only small fraction of those information is needed, including some simple dimensional details and slight understanding of the AM machine and the material objected to be used for the manufacturing process [26]. The general principles for all AM machines are the same; they all use same approach called the layer-by-layer technique.

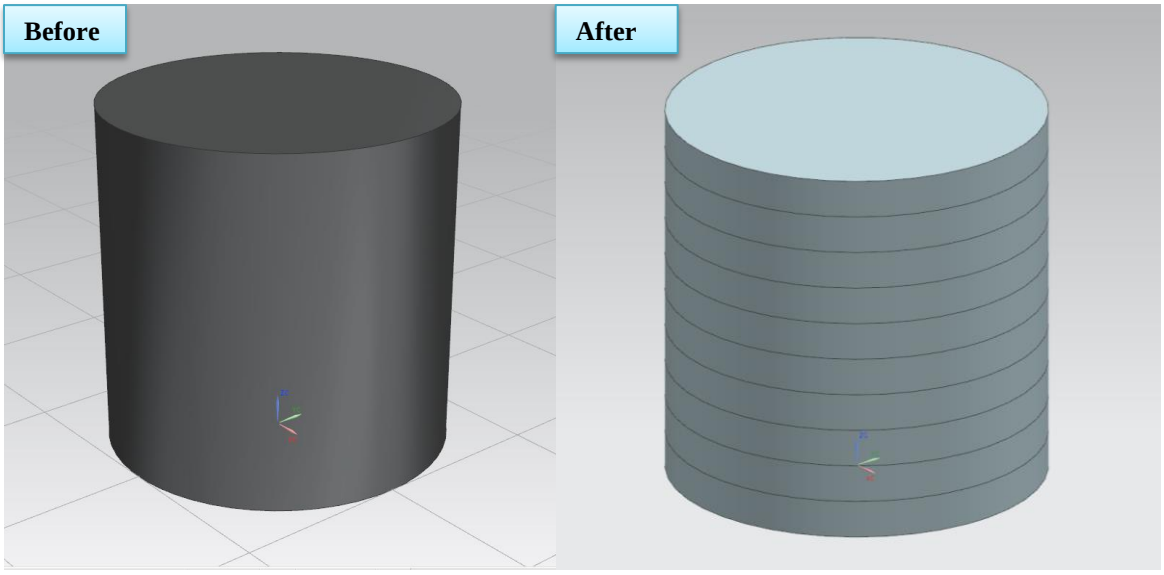

Figure 1. 3D CAD design of a cylinder before and after feeding to the AM machine

In additive manufacturing processes a three dimensional Computer Aided Design (CAD) of the desirable part will be generated using a 3D CAD software. Then that 3D model will be fed to the AM machine; pre-processing software slices the image into layers, which are then converted into machine-specific parameters and trajectories for generating each layer. And at last the additive manufacturing system creates the part bay generating those layers one by one on top of each other until the part is completed. The thickness of these layers is very important due to their direct effect on the quality of the final product. In order to generate a part as close as possible to the original 3D CAD design, the slices need to be as thin as possible. For example, in Figure 1, the image on the left is the 3D CAD design of a cylinder that is going to be manufactured by an AM machine. Then when it is fed to the machine, it will be sliced into equal layers.

In general additive manufacturing could be broken down into eight steps including [26, 52]:

1. Conceptualization and CAD modelling
2. Conversion to STL file
3. Transferring STL file to the manipulator and AM machine
4. Machine Setup
5. Construction sequins
6. Part removal and cleaning
7. Post processing

8. Application

Even though almost all of the AM systems follow these general steps, it doesn't mean these eight steps are exactly the same for every individual AM machine. Except the first two steps, the rest depends on what technology will be used to create that particular design of the desirable part; it may also depend on the actual geometry of the part and the material as well.

2.3 Additive Manufacturing Techniques

Currently there are many different AM machines that have been commercialized and even though all of them use the same general principle (layer-by-layer) to operate, there are few ways that they could be differing from each other. The first element would be the material; each type of AM machines can only operate with certain range of materials. The second element to differ one AM machine from another is how the machine creates the layers. And at last, each type of AM machines uses a different method to bond the layers together. Table 3 shows an overview of the AM family from past till present; this table was originally gathered by Kruth et al. [53].

Table 3. The chain of additive manufacturing according to Kruth et al [53].

Supply	Process	Layer creation technique	Phase change during layer solidification	Materials	Variants/Laser based
Liquid	Stereo-Lithography (SLA)	Liquid layer deposition	Photo-polymerization	Photo-polymers: • Acrylates • Epoxies • Filled resins: (glass, ceramic, metal,…)	Laser illumination Flash lamp + milling layers
	Fused Deposition Modelling (FDM)	Continuous extrusion and deposition	Solidification by cooling	Polymers: (ABS, PA, ...) Wax Filled polymers (glass, …)	FDM
				Metals with binder	MJS
				Ceramics with binder	FDC
	Ink Jet Printing (IJP)	Drop-on-demand deposition	Solidification by cooling	Polymers wax	 Milling layers 5-axis milling layers + contour
Powder	Three Dimensional Printing (3D-P)	Layer of powder+ Drop-on-demand binder printing	No phase change	Ceramics with binder Metals with binder Polymers with binder	
	Selective Laser Sintering (SLS)	Layer of powder	Laser sintering/ Laser melting& solidification by cooling	Polymers: (PC, PA, …) Filled polymers: (glass, …) Metals with binder Metals:(pure) Sand, ceramics	Laser-based
	Laser Cladding	Continuous injection of powder	Laser melting& solidification by cooling	Metals	Laser + milling layer and contour Laser-based
Solid	Laminated Object manufacturing	Deposition of sheet materials	No phase change	Paper	Laser cutting Knife cutting
				Polymer	
				Polymer foam	Heated wire cutting
				Composites	Laser cutting
				Ceramics	
				Metals	
Gas	Selective Laser Chemical Vapour Deposition	Condensation of gas	Forming solid from gas by chemical reaction	Metals: (Al, FeNi, …) Ceramics: (Sic, …)	Laser-based

In Table 3, three dimensional printing (3D printing) and ink jet printing (IJP) have been separated but they are almost the same. Most likely Kruth et al categorized them separately because of the material. Frequently it has been refer to 3D printing as ink jet printing or binder jetting [54, 55]. By looking at Table 3, it is easy to say that there are numerous types of AM systems capable of different applications using diverse materials. But, some of these systems are less popular than the others. When it comes down to biomedical application SLA, SLS, and 3D Printing are the most popular AM systems commercially available.

3D printing systems have an advantage compare to SLA and SLS techniques; the absence of laser usage in this method makes it more user friendly and less complicated; 3D Printing will be described in more detail in the next section.

2.4 Ink Jet Printing/3D printing

Cima MJ and Sachs et al. are credited with invention of 3 Dimensional Printing (3DP) and patented it (US Patent US005340656A) in the year 1993 [56], and it was based on the conventional inkjet printing technology [57]. 3D printing systems are powder based. The process involves spreading thin layers of powder on top of each other and bonding those layers by depositing stream droplets of an adhesive liquid binder over the surface of each layer. The process of stacking layers on top of each other will continue till the part is completed.

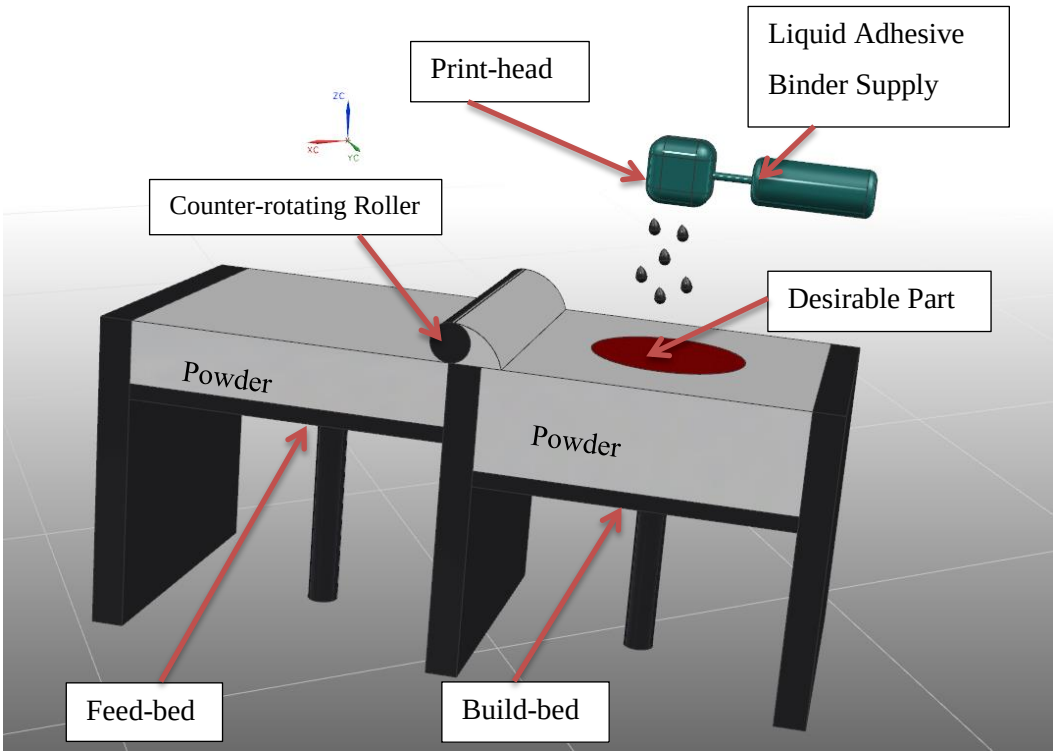

Figure 2. General components of a 3D printer

As previously mentioned, AM systems follow eight general steps; here those steps will be explained in more details in the context of 3DP. For example, Figure 2 shows a basic 3D printer that is printing a half sphere; the eight steps from start to the final product (half sphere) will include:

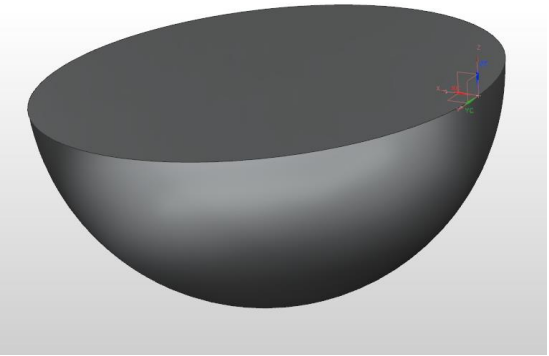

Figure 3. Three dimensional CAD model of a half sphere

Step-1: At this stage, the idea and a concept of the half sphere will be transformed to a sketch and representative 3D model. In order to do this, CAD software will be used to generate a 3D model using a computer, similar to Figure 3.

Step-2: The 3D CAD model has to be converted to an STL file which allows a simple way of expressing that CAD model in terms of its surface geometry [26]. The first commercial AM technology from 3DSystems in the 1990s was called StereoLithography which is where the STL term comes from [26]. Almost all of the current CAD software has the conversion to STL option built-in. When generating the STL model, the surfaces of the part are approximated with series of tiny triangular planes [26, 52].

Step-3: After generating the STL file, it is time to feed that file directly to the interface of the 3D printer. Every AM machine has a different interface, but almost all of them have a visualization tool; in this case when the STL file was sent to the 3D printer, it should be easy to look at the part using the visualization tool. This tool would help to verify that the part is correct and it's visually same as the intended 3D CAD model. It is also possible to build multiple parts at a same time, copies or completely different design, and in this scenario the visualization tool would also be able to help the user to relocate the parts or change the orientation of those parts. The STL files are also linearly scalable. It means depending on the application of the part, the user may require making the part slightly bigger or smaller which again user should be able to do so within the AM machine interface.

Step-4: After making sure that the STL file has been transferred to the 3D printer and all visual aspect of the design are same as what was meant to be, the final settings to start the

build are implemented. The final settings would be the machine set-up. Every AM machine has a unique set of building parameters that could be changed. Material type, environmental temperature, compensation factors, layer thickness and binder concentration are the main parameters that can be changed in a 3DP machine set-up. Often, the anticipated machine has a list of materials that one can be chosen from to operate on or one new custom material can be added to that list by entering some of the properties or some specific details that the machine will require; then by choosing one of those options the machine will save some default settings that are necessary in order to operate with that particular material type. 3D printers are powder based so when you select a material, it might ask you about the particle size as well. Layer thickness is another parameter that can be changed by the user; layer thickness effects the time of building operation. The thicker the layers are the shorter period of time needed to 3D print a part. 3D printers are usually compatible with more than one liquid binder depending on the powder material that is going to be used. Some machines allow you to change the amount of the binder that it gets sprayed on the powder. In some cases that could be a good thing and lead to save some binder for the next print; however, by changing the binder saturation levels or layer thickness, the quality and integrity of the final product might have been compromised.

Step-5: After selecting the preferable settings in the machine set-up, the part can then be printed. The 3D printer will follow the same basic principle that was mentioned earlier, in layer-by-layer printing. The easiest way to describe the process is by looking at Figure 2. In 3DP there are two main chambers that each has a bed, one is called the feeding bed and the other is building bed. Both beds move proportional to each other. At the beginning the

feeding chamber is filled with powder, when the print starts the building bed goes down one increment and the roller moves to the far left side behind the feeding chamber, then the feeding bed moves one increment up and next the roller will spread the powder from left to the right side over the building bed. After the powder was spread on the building bed the print head comes and prints a 2D cross section of the part. Then the same cycle repeats till the part is finished.

Step-6: After the print is over, the part can be removed from the chamber. In figure 2, the part is a half sphere but it looks like a 2D circle from the top. Figure 4 is a cross section image of the same 3D printer and it shows the rest of the part (half sphere) is under the powder.

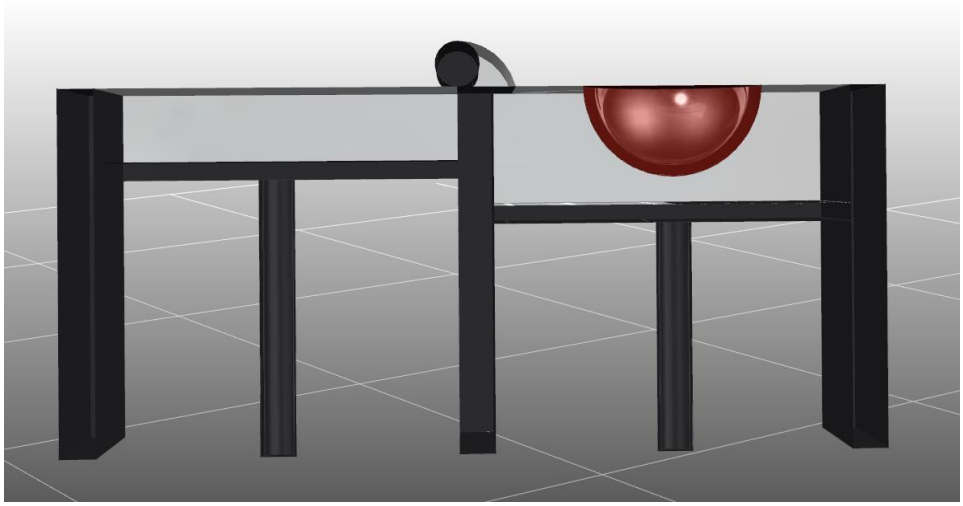

Figure 4. The cross section of building and feeding bed of a 3D printer at the end of the print of a half sphere

After the part has been removed it can be cleaned using a tool like an air blower or a brush depending on how sensitive the part or the material is and proceed to the next step.

Step-7: This step totally depends on what type of application the part has been made for. Sometimes the part is just for some visual concept evaluation and does not require a post processing other than the cleaning that was done before. In some cases depending on the material the part might have a more practical role and it needs to be strong by curing its particle bonds, so it needs to be thermally treated in a furnace using a specific protocol. In some other scenarios post processing could involve smooth finishing, like polishing or coating[26]. Other post-processing may involve polymer infiltration.

Step-8: At this stage the part is ready use for the suited application. However depending on how critical the rule of the part is, some additional inspections could be a good idea to assess the part and compare it with the require standards.

2.4.1 3D Printing Ceramics and the Interest toward Bone Tissue Engineering

In the year 1993, it was the first time that ceramic powder was used for 3D printing [26]. Yoo J et al used alumina powder for the process and latex binder to print on it; the reported fired alumina parts were more than 99.2% dense and reached a flexural strength of 324 MPa at the time [58].

Few years later, Giordano et al reported using a biodegradable polymer called Polylactic acid for 3D printing [59]. The report provided evidences showing successful 3D printing of dense polymer parts with appropriate strength; which allowed producing complex structures with a range of microstructures within the same part [59].

More researchers have started investigating the use of 3D printing toward bone tissue engineering, typically using ceramics and ceramic composites. In the past decade, significant

number of papers has been published reporting that 3D printing was used on different bioceramics including β-TCP, TCP, α-TCP, Bioglass, HA, and CPP toward bio applications [3, 6, 60–68].

Pre-processing the powder might be required when bioceramic powders are being used; often the powder is being mixed or coated with another polymer that can dissolves when exposed to the printed liquid binder and act as a glue to improve the green part (non-sintered part) strength [45]. Better packing, flowing and wetting behavior are another results of the powder's pre-processing which will also lead to have improved high geometrical resolution for controlled pore structure formation [3].

3D printing is often preferred to other conventional manufacturing techniques when it comes to bioceramics. Computer numerically controlled (CNC) machining is one of those commonly used manufacturing techniques that is losing its place to 3D printing in bioceramic; it has considerable amount of waste and it is quite time consuming compared to 3D printing. Furthermore, when it comes to ceramics or other brittle/porous materials, the cutting forces of CNC machining might cause hidden micro cracks on the construct which might weaken the mechanical strength and the durability of the part [9].

AM techniques such as 3DP have the capability of fabricating complex shaped implant designs to be tailored and fit patients sophisticated tissue defects using computer tomography (CT) scanning and magnetic resonance imaging (MRI) [15, 68, 69]. 3D printing allows you to generate small feature, with feature size depending on particle size and layer thickness or

complex feature like curved channels which is not possible using CNC machining [16, 57, 70]. Table 4 is a summary of the advantages and limitations of 3D printing.

Table 4 3D Printing: advantages and limitations [4, 9, 15, 16, 57]

Three Dimensional Printing (3DP)	
Advantages	**Limitations**
• Easy process • High porosity • High surface area to volume ratio • 100% pore interconnectivity • Macro shape control • Diverse range of materials • Independent control of porosity and pore size • No support structure required • Cost efficient • Achievable pore size: 45-150 μm • Build accuracy: down to ±0.02 mm	• Poor mechanical strength depending on the material • Limited to small pore sizes • De-powdering difficult, especially in closed, complex, or small cavities • Homogeneous material properties throughout the part in terms of micro porosity and material composition

Gravity sinter processing is a conventional technique that has been used to manufacture CPP parts. Based on the work by Shanjani et al. using 3D printing to manufacture CPP parts

[71], there was a second study carried out by Hu et al comparing both methods together which stated an increase from 21 ± 4.5 MPa for conventionally fabricated CPP samples to 50.2 ± 4.74 MPa for 3D printed CPP parts in their compressive strengths [23]; The studies carried out by Shanjani et al. and Hu et al. suggested that 3D printing can replace conventional manufacturing techniques when it comes to manufacturing CPP parts with higher mechanical strength. There is a possibility to improve the mechanical properties even further by changing some of the process parameters in 3D printing. One of those parameters would be the powder material particle size. By using smaller and finer powder particle size, thinner layers can be printed which could lead to better surface quality, better mechanical strength, and more dense parts. However, in the case of 3D printing ceramics, fine powder does not intend to flow well enough to be spread by the counter-clockwise rotating roller when using dry powder. This study is about 3D printing fine CPP powder (< 75 μm) and improving mechanical and structural properties of bone substitutes.

2.5 Summary

This chapter briefly explained the benefits of biodegradable implants and the influence of additive manufacturing techniques in the biomedical industry. It was described how biodegradable materials have shown great potential and many advantaged in comparison with the old fashion metallic materials in the biomedical industry. Following that, the concept of additive manufacturing techniques were briefly explained; more specifically 3D printing technique was described in details including how it has started to merge with bone tissue engineering. Calcium polyphosphate was one of those biodegradable materials which have shown promising results over the past decade in bone tissue engineering. CPP was

subjected to 3D printing and the results have shown significant improvements compare to the previous manufacturing technique. It was also explained, overcoming some of the current limitations in 3D printing including poor flow behavior in the fine dry powder could lead to a better final product with improved properties. In this study, a fine CPP powder with a particle size of < 75 µm was subjected to 3D printing and for the first time a new solution was suggested to improve the flow behavior of the fine CPP powder. In the next chapter, the methods used and necessary steps taken are explained in details.

Chapter 3
Methodology

This chapter defines studies on the additive manufacturing (AM) of porous Calcium Polyphosphate (CPP) structures by using porogens substrate to print on fine powder. Details and specifics of each individual step taken through the whole process are addressed; beginning from the first step material and preparation methods, through the AM process, after processing, and at last every examination process that was taken to characterize the manufactured samples.

3.1 Materials and Preparation Methods

3.1.1 Materials

In this study, CPP and Polyvinyl Alcohol (PVA) were the only powder material that was used for the AM process. The main material was CPP for being the point of interest candidate for bone synthetic substitute biomaterial and PVA was consumed as a sacrificial bonding agent in the AM process.

As it was described earlier in Chapter 2, the CPP powder is produced by a dehydration process showed in the equation (1).

The team at the University of Toronto was responsible for producing CPP powder and the powder is prepared in two particle sizes including CPP 75-150 μm and CPP < 75 μm. In this study the fine CPP powder (< 75 μm) was used. The only liquid material in this study is the aqueous solvent Zb^{TM}58 (Z Corporation, Burlington, MA, US) which was used to inject

on the powder during the AM process. After receiving CPP powder from the University of Toronto, it was mixed with PVA through a specific procedure as described below.

The PVA was purchased from Alfa Aesar (Alfa Aesar, Ward Hill, MA, USA). However, based on the previous CPP studies, the PVA needs to be grounded to a smaller particle size (< 63µm) before mixing with CPP. The grounded PVA was sieved to <63µm using a sieve No. 230 and a D-4325 sieve shaker made by DUAL Manufacturing (Dual Manufacturing, Franklin Park, IL, USA) was used to speed up the process instead of shaking the sieves manually using hands.

After preparing the PVA fine powder in order to make the base powder so called "Bulk powder" for 3D printing, the CPP and 10 weight % PVA were mixed according to the equation (2), for 5 hours on a roll jar mill (US Stoneware, Ohio, US) . The 10% PVA is to provide sufficient green part strength and this was based on the previous investigations done on CPP [9, 15].

$$Bulk\ Powder = 90\%(CPP < 75\mu m) + 10\%(PVA < 63\mu m) \quad (2)$$

3.1.1.1 Liquid Material

The only liquid material used in this study was the adhesive binder that was dispersed on the powder substrate during the 3D printing process. Two aqueous solvents Zb58 and Zb60 (Zb ^{TM}58, Zb ^{TM}60, Z Corporation, Burlington, MA) were the two liquid binders used to print on the CPP-PVA powder.

3.1.1.2 Porogens

Previous studies shown that the large particle CPP powder (75-150 µm) had no problem during AM process including the flowability. Considering this point, in order to improve the flowability, it was decided to use some percentage of a large particle size powder mixed with the fine powder CPP. The large particle size powder was decided to be PVA 75-106 µm and this decision was based on a number of reasons including:

- Other than improving flowability, the large particle PVA could mean additional pores and that is why the term "porogen" was given as the name.
- PVA was used as porogen because it did not required second investigation to be proven as process friendly for using with CPP.
- 75-106 µm is within the size range of large particle CPP (75-150 µm) which had no flowability issues.
- Porogens can be separated from the bulk powder easily only by sieving the powder through a sieve with a pore opening size of 75 µm.

For each experiment a different percentage of porogens was added to the bulk powder and mixed for 5 hours on the jar mill (Figure 5).

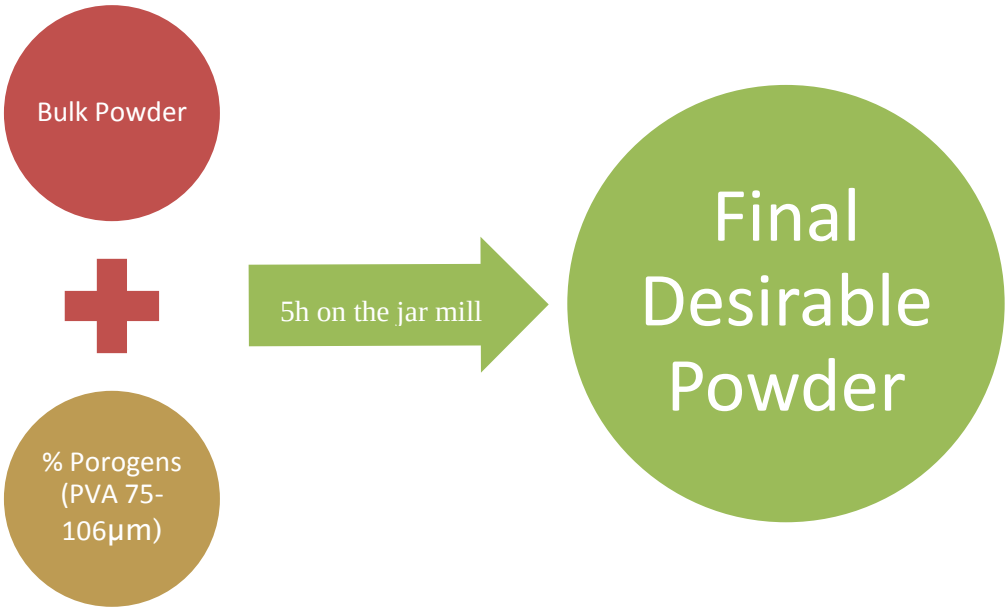

Figure 5. Powder mixing process for each experiment

3.2 3D Printing Porous CPP Structures

3.2.1 CAD Model

The AM process starts with 3D modeling of the desired geometry using CAD software. In this study, SolidWorks Ver2012 (SolidWorks Corp.,Concord, MA, USA) was used as a standard CAD package to interpolate the design of the CPP structure.

Based on the previous studies done by Shanjani et al. and Vlasea et al., cylindrical shaped implants were chosen as the desirable geometry which were 4mm in diameter and 6mm in height[9, 15, 71]. The 3D model of the cylindrical shaped implants were made using SolidWorks and then was exported in the StereoLithography (STL) format so it can be uploaded to the 3D printer.

3.2.2 Machine Set-up

In this thesis, a Zprinter 310plus (Z Corporation, Burlington, MA, US) was used as the 3D printing machine to fabricate the porous CPP parts by the mean of layer-by-layer technique.

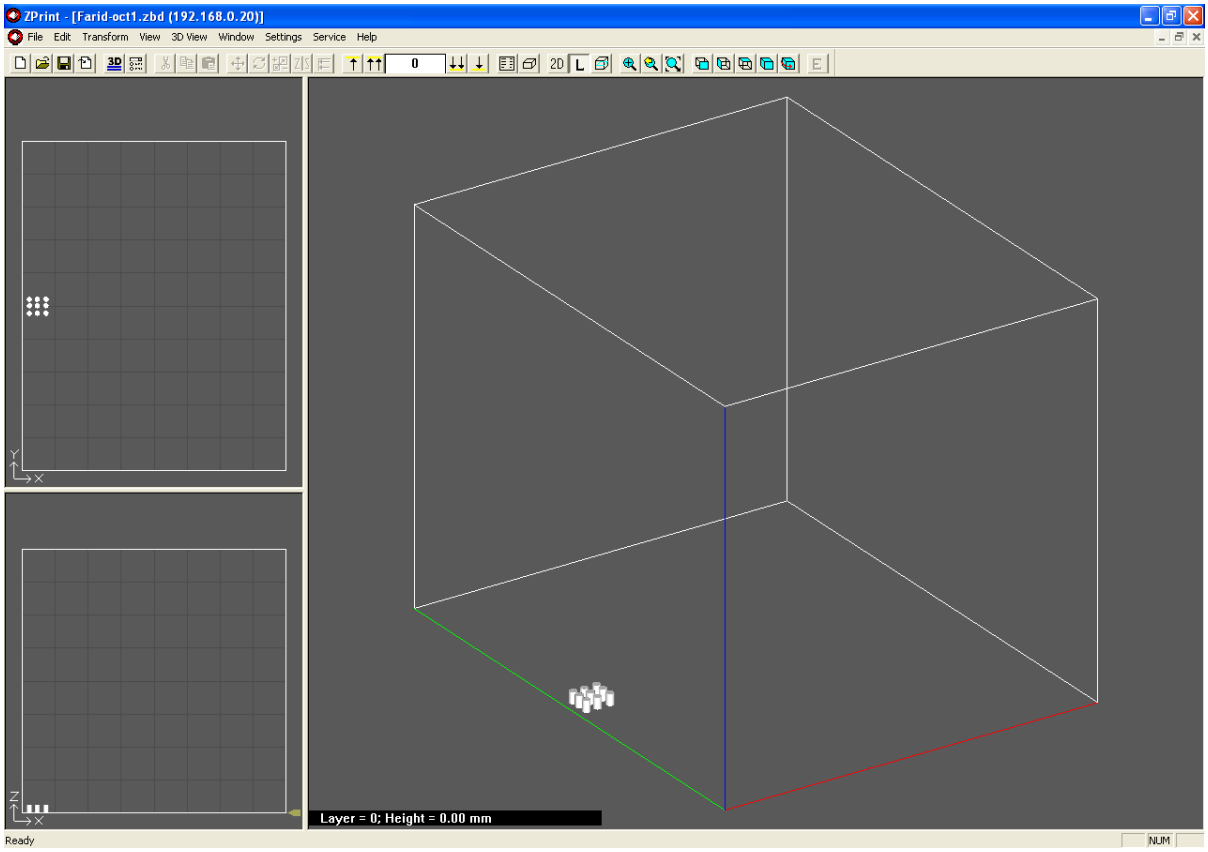

Figure 6. 3D printing software visualization interface Zprint™

After generating the STL file, it was then uploaded to the machine's software (Zprint™) which takes the 3D model and processes it into 2D slices. The software has a visualization tool which is capable of showing the uploaded STL file; in that environment the user can check the part and if needed alter few things including the part location, orientation,

or adding multiple parts. Figure 6 shows the visualization interface of Zprint™, and it can be seen that the cylindrical implants were multiply by 9 for each print (3x3).

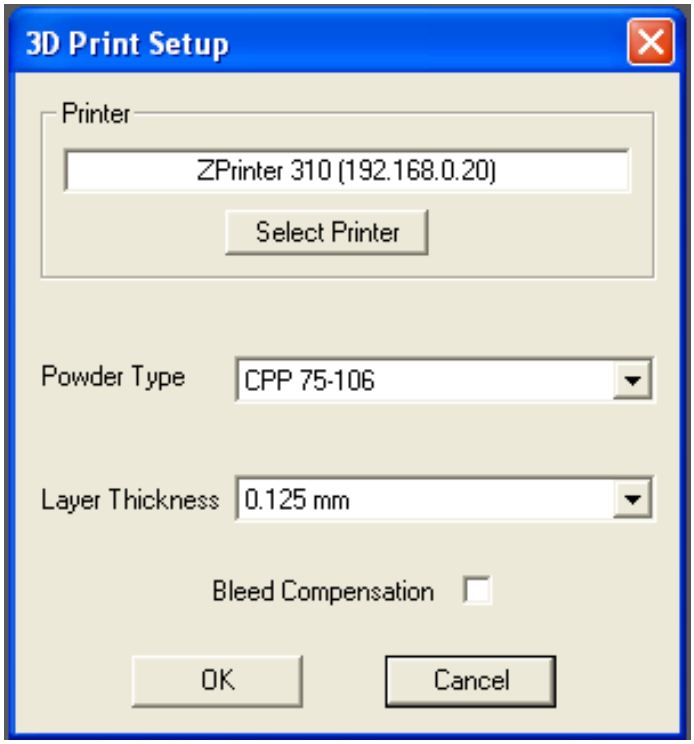

Figure 7. 3D print Set-up: powder type and layer thickness

After making sure visually everything was at the right place, the final step before printing had to be setting the layer thickness. A new powder type was introduced as "CPP 75-106" with a layer thickness of 0.125 mm (Figure 7). It was mentioned earlier that the thinner layers could mean better surface quality, however the layer thickness cannot be smaller than the largest powder particle size. In this case the powder is a mixed of two different material type, the largest CPP powder particle size is 75 µm and the largest PVA powder particle size is 106 µm (porogens); this means the layer thickness has to be bigger

than 106 μm and that is why the closest layer thickness was chosen from the machine set-up to be 125 μm.

3.2.3 Additive Manufacturing

After the machine set-up was complete, the machine would start to build the part one layer after another. As described earlier in Chapter 2, in the AM process, the counter-rotating roller would collect the powder from feeding chamber and spread it over the building chamber; then the print head would come over the top of the building chamber and a 2D image of each layer gets printed on the CPP-PVA powder which in this case due to the printing orientation that image was a 2D circle (9 circles because 9 cylindrical parts were printed together in each build, Figure 6). Same process was repeated and layers were stacked up on top of each other for about 15 to 20 minutes till the parts were completed.

3.3 Post Processing and Sintering

3.3.1 Part Removal and cleaning

The CPP green parts (non-sintered parts) are weak, especially after the printing process is over; and that is why the parts are left in the building chamber for at list two hours to be dried out. Then the parts that dried out for a while were taken out and got de-powdered individually using a small plastic brush.

3.3.2 Heat Treatment

Each cylindrical CPP green part that was de-powdered had to be measured in both diameter and height. After dimensional measurements of green parts, they were packed and

shipped to University of Toronto for sintering. The sintering process consists of two main parts including:

I. Getting rid of the polymeric binder by burning it off.

II. Using the two step protocol that was patented to densify the CPP powder [12].

The whole process has been shown in details in the Figure 8; the burn-off process of polymeric binder has been highlighted as green in the Figure 8 and the rest of it presents the two step protocol for densifying CPP powder.

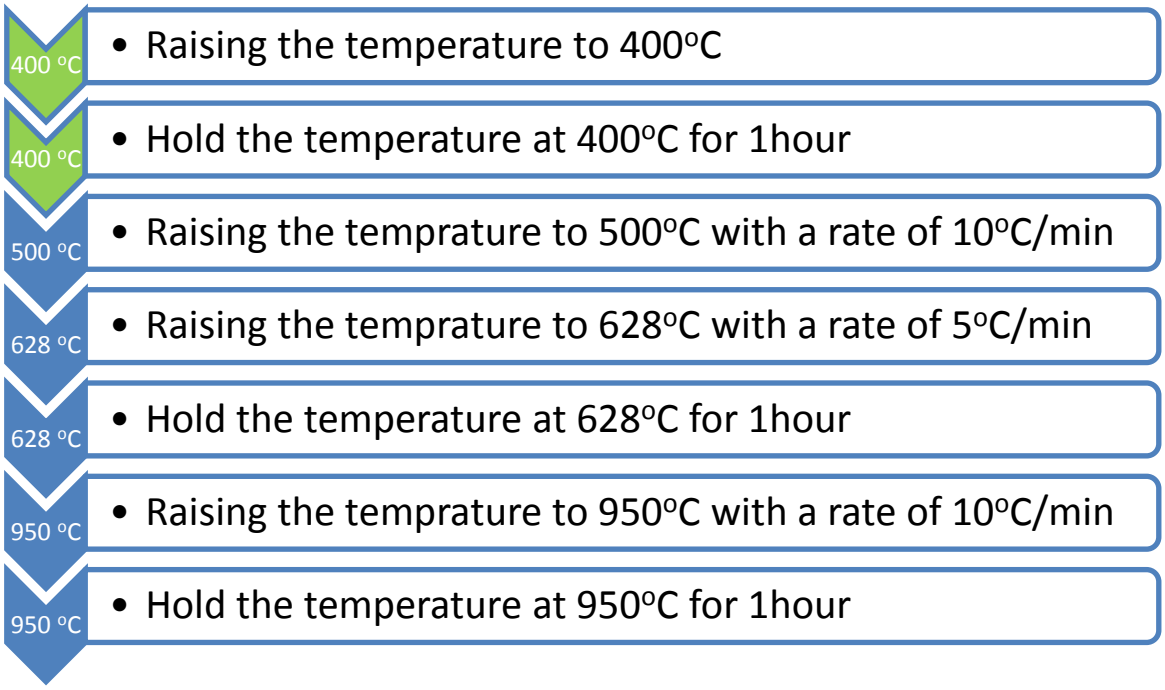

Figure 8. The sintering protocol for the after processing the 3D printed CPP green parts [12]

After the sintering was done, the manufacturing process is complete and the CPP structures were ready for characterization.

3.4 Characterization of Sintered Parts

When the sintered parts were ready, in order to evaluate the process and out-coming results, the sintered CPP structures had to undergo 4 characterization steps. Those steps in the order from first to last include: shrinkage measurements, porosity measurements, compressive strength assessments, and at last SEM.

3.4.1 Shrinkage measurements

Before anything was done to the sintered CPP parts, the diameter and the height of the sintered CPP cylinders had to be measured. A digital caliper (Absolute-Digimatic, Mitutoyo Corp., Japan) was used to measure those dimensions and then the readings were recorded and compared with green part dimensions for shrinkage analysis using the equation (3) below.

$$Shrinkage\ (\%) = \frac{x_{green} - x_{sintered}}{x_{green}} \times 100 \quad (3)$$

- x_{green} is the dimension measured (height or diameter) before sintering (green part)
- $x_{sintered}$ is the dimension measured (height or diameter) after sintering (sintered part)

3.4.2 Porosity Measurements

The second step in the characterization process was porosity measurements. The ethanol displacement which is based on Archimedes principle was used to determine the

porosity for each sintered CPP cylinder. First, the dry mass (M_{dry}) of each sample was stablished using a precision micro-scale balance (APX-203, Denver Instrument, Bohemia, NY, US); after measuring the dry mass, all of the samples were individually immersed in ethanol and then sonicated (VWR Ultrasonics Cleaner B2500A-DTH, VWR International, West Chester, PA, US) for 45 minutes at 30°C. Afterward, using the bath kit, each sonicated specimen was suspended in ethanol individually and the mass suspended (M_{susp}) was measured. Subsequently, the suspended sample was removed from ethanol to be quickly tapped with a lint free fabric to remove glut ethanol and then was weighed right away to establish the wet mass (M_{wet}). The equations (4) and (5) were used to calculate the bulk porosity:

$$\rho_{bulk} = \rho_{ethanol} \times \frac{M_{dry}}{M_{wet} - M_{susp}} \tag{4}$$

$$P_{bulk} = \left(1 - \frac{\rho_{bulk}}{\rho_{CPP}}\right) \times 100 \tag{5}$$

- ρ_{bulk} is the bulk density
- $\rho_{ethanol}$ is the density of ethanol considered to be at the room temperature (0.785 g/cm^3) [13]
- ρ_{CPP} is the theoretical density of non-porous CPP (2.850 g/cm^3) [13]

3.4.3 Compressive Strength Assessments

Each category depending on each experiment was populated with *n* = 6-15 cylindrical samples with a layer thickness of 125 µm. Uniaxial compression test was applied to all of the

specimens which were 4mm in diameter and 6mm tall. The compression test was performed using a calibrated 1 kN load cell with a loading rate of 0.2 mm/min (Instron 5548 Micro-Testing, MA).

3.4.4 Statistical Analysis

Shrinkage, porosity, and compressive strength results are described as averages with the standard deviations.

The equations (6) and (7) also known as the Weibull distribution was applied to calculate the probability (P) of failure of the porous CPP parts at or below a stress (σ) and to demonstrate a statistical means of evaluating the distinction of the experimental results [15, 72–74].

$$P(\sigma) = 1 - \exp\left[-(\frac{\sigma}{\sigma_o})^m\right] \quad (6)$$

$$P(\sigma) = 1 - \frac{(i - 0.3)}{(n + 0.4)} \quad (7)$$

- P is the failure probability
- σ_o is the Weibull characteristic strength
- m is the Weibull modulus
- n is the population of samples
- i is the related rank of the sample measurement

3.4.5 The Dynamic Flow Properties and the Mean Powder Particle Size

Three different powders were sent to ATS Scientific laboratory (ATS Scientific Inc., Burlington, Ontario, Canada) to be tested in order to determine the flowability of each powder and the mean particle size.

A machine called FT4 Powder Rheometer (FT4 Powder Rheometer, freemantechnology, Tewkesbury, England) was used to establish the Basic Flowability Energy (BFF). The way this machine operates is by moving an anti-clockwise precision rotating blade down a helical path through the desirable powder; then the BFF is determined from the work done in stirring the blade through powder from the top to the bottom of the powder vessel. Another machine called Horiba LA960 (LA960, Horiba Scientific, Kyoto, Japan) was used to establish the mean particle size for different powders; the LA960 uses laser diffraction to determine the particle size.

3.4.6 Scanning Electron Microscope (SEM)

In order to observe the microstructure of the cylindrical CPP parts, a number of samples with different percentages of porogens were chosen to be observed by scanning electron microscope (SEM; JSM-6460, Jeol, Akishima, Tokyo). Before performing SEM imaging on CPP specimens, samples had to be sputter-coated with a 10 nm thick gold layer (Desk II, Denton Vacuum, LCC, Moorestown, NJ, USA) to be electrically conductive; then the machine was at 20 kV accelerating voltage to start the imaging process.

3.5 Summary

The pre-processing procedure included powder grinding, sieving and mixing. The bulk powder was first created by mixing the fine CPP powder (< 75 μm) and the fine PVA powder (< 63 μm), then mixed with needed percentages of porogens (large particle PVA 75-106 μm) to make the final desirable powder for AM process. Following the pre-processing, the final powder was subjected to the AM process. The CAD model was converted to a STL file and then loaded to the AM machine's software. After making sure that everything was visually fine at the right place, the layer thickness was set to 125 μm and then the building process was started. After the AM process was finished, the finished cylindrical CPP parts (green parts) had to go through a post-processing procedure which included cleaning/de-powdering, and the heat treatment protocol. Following that, when the parts were sintered the production was completed and they had to be characterized through different examination processes. The characterization methods included shrinkage measurements, porosity measurements, compressive strength assessments, statistical analysis, the dynamic flow properties and the mean powder particle size, and SEM.

Chapter 4
Results and Discussion

This chapter mainly consists of three main experiments. Experiment 1 was the key experiment; Experiments 2 and 3 were the follow up experiments to Experiment 1. After Experiment 1, the liquid binder Zb58 was finished and had to be replaced with Zb60 because it was no longer at production. As a result, it was decided to do a second experiment (Experiment 2) and repeat some of the categories in the Experiment 1, to see if the results from Experiment 1 can be achieved using Zb60. Experiment 3 had only two main categories repeating best results in the previous experiments. The categories in each experiment were differing from each other based on the powder that was being used to additive manufacture parts; each powder had a certain percentage of porogens particles. Figure 9 describes each experiment and the corresponding categories.

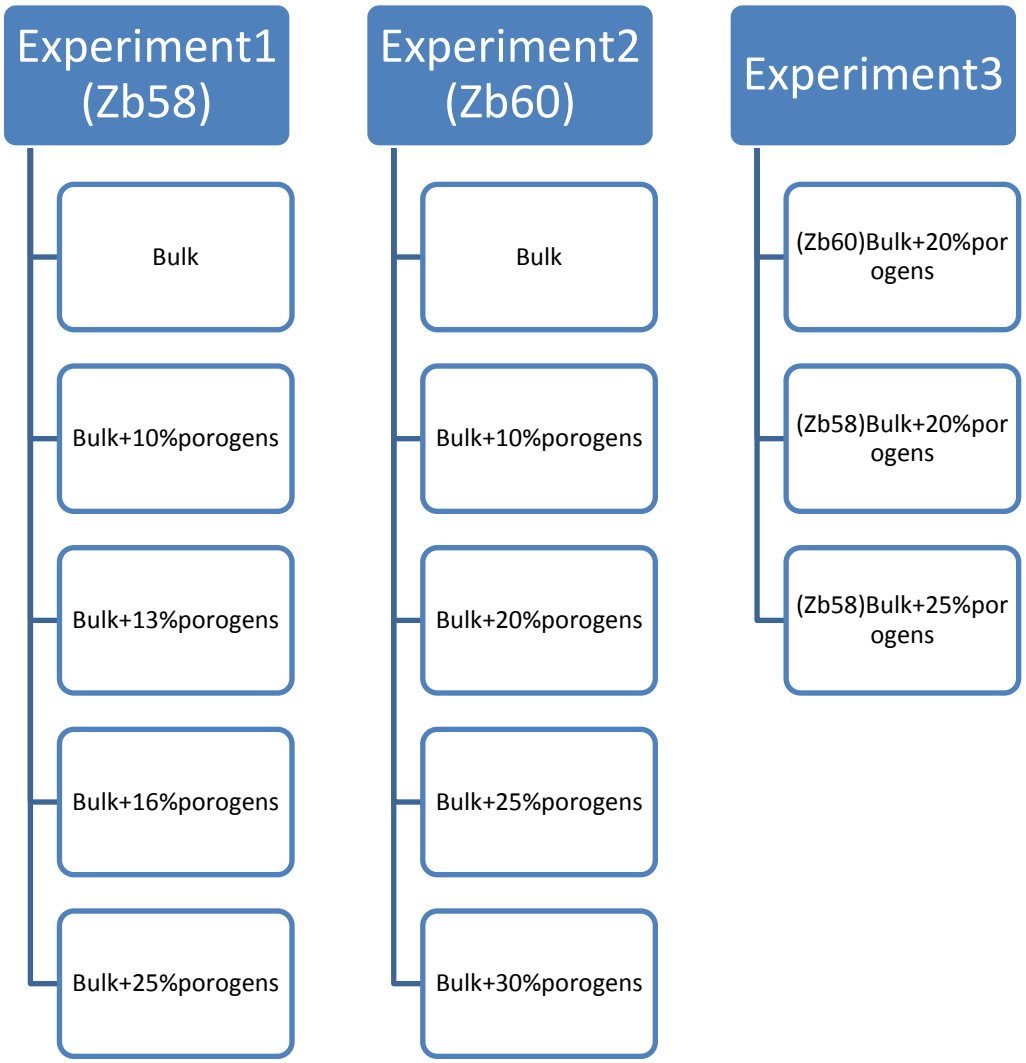

Figure 9. The three experiments and the categories within

4.1 Results

4.1.1 The Powder Flowability and The Average particle size

Three different powders were sent to ATS Scientific laboratory including:

- Powder 1: Bulk powder (90% CPP < 75 µm+10% PVA< 63 µm) (green line, Figure 10)

- Powder 2: Bulk powder +25% Porogens (blue line, Figure 10)
- Powder 3: Large particle bulk powder (90% CPP 75-150+10% PVA < 63 µm) (pink line, Figure 10)

Powder 3, was the one that was used in almost all previous studies related to AM processing of CPP powder.

All three powders were tested using two different machines. The first machine, Horiba LA960, was able to identify the average particle size for each powder; in Table 5 as predicted, powder 3 had the largest average particle size and the other two powders had almost the same average particle size.

Table 5. Average CPP particle size for powder1-3 obtained by Horiba LA960

	Powder 1	**Powder 2**	**Powder 3**
Average CPP particle size (µm)	41.27	42.76	110.14

The second machine FT4 Powder Rheometer was used to establish the flow behavior of all three powders. The results have been shown in Figure 10, according to the report a higher total energy indicates better flowability which in this case powder 3 had the best flowability and powder 1 corresponded to the worst one.

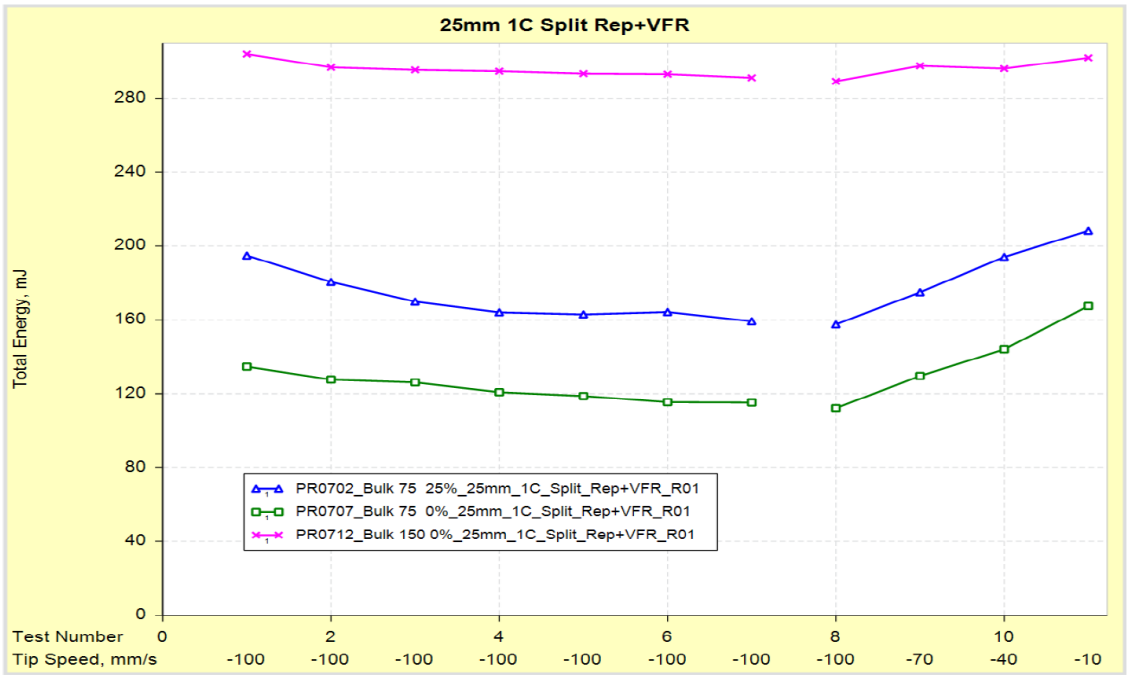

Figure 10. Flowability energy as a function of repeated tests and flow rate change

The details of the powders characteristics that were reported by ATS Scientific Inc. are tabulated in the appendix.

4.1.2 Dimensional Shrinkage

The CPP parts are expected to shrink after the sintering protocol was applied [6, 15, 71]. The diameter and the height were measured for every individual AM produced CPP samples before and after sintering; then the equations mentioned in subchapter 3.4.1 was used to calculate the shrinkage percentage of each sample. The results for individual categories within each experiment are summarized in Table 6. In each experiment, the category with highest percentage of porogens had the highest shrinkage percentage in both height and diameter.

Table 6. The average dimensional shrinkage (%) in diameter and height for three experiments, each experiment had different categories based on the different percentages of porogens. Empty cells simply indicate the absent of that category (or categories) in the corresponding experiment.

	Experiment 1		Experiment 2		Experiment 3	
	Diameter	Height	Diameter	Height	Diameter	Height
Bulk Powder	11.4%±4.2	15.2%±2.9	12.8%±5.4	15.5%±3.7		
Bulk Powder+ 10% Porogens	23.2%±2.4	24.4%±3.6	17.3%±1.7	21.1%±1		
Bulk Powder+ 13% Porogens	21.6%±2.2	24.7%±1.9				
Bulk Powder+ 16% Porogens	25.1%±1.2	26.9%±0.7				
Bulk Powder+ 20% Porogens			22%±1.4	25.4%±0.9	20.6%±3.5	21.2%±1.7
					23.1%±1.7	22.8%±1.3
Bulk Powder+ 25% Porogens	27.8%±1.3	28.1%±4.2	24.5%±1.2	28.1%±1.9	22.3%±1.6	23.5%±1.8
Bulk Powder+ 30% Porogens			28.2%±3.2	34.4%±0.8		

4.1.3 Bulk Porosity

As it was mentioned earlier in the subchapter 3.4.2, the Archimedes principle was used to calculate the bulk porosity. The parts that were additive manufactured using the bulk powder with 30% porogens, were not acceptable and did not go through the rest of the

characterization process after the shrinkage analysis. The bulk porosity was calculated for 175 cylindrical CPP part throughout Experiments1-3.

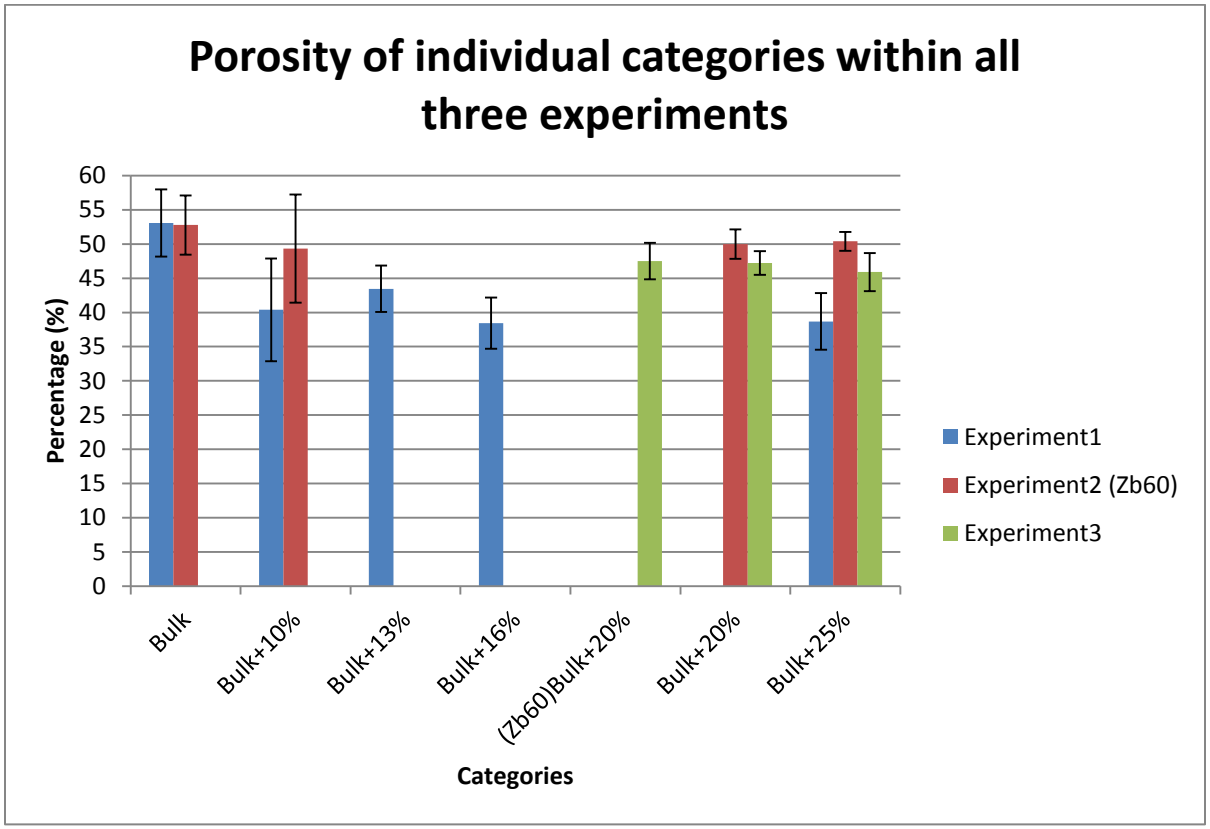

Figure 11. The average bulk porosity for individual categories for all three experiments, except the one with 30% Porogens.

In Figure 11, for Experiments 1 and 2, the difference in porosity percentage between the category with no porogens (bulk) and the category with 25% porogens is quite clear; however, this difference in Experiment 1 is more significant. Furthermore, the bulk category has the highest porosity percentage between all categories within all experiments.

4.1.4 Uniaxial Compression Results

The compression test results for additive manufactured CPP cylinders are shown in table 6. All of the specimens were fabricated using the same AM machine and the layer thickness of 125 μm; except Experiment 2 and one category in Experiment 3, the rest of CPP cylinders were made by dispersing Zb58 as the liquid binder.

Table 7. Compression test result parameters for samples within all three experiments

Experiment 1			
	Stress (MPa)	Strain (mm/mm)	m(R^2)
Bulk Powder	11.53±2.99	0.04±0.001	3.37(0.84)
Bulk Powder+ 10% Porogens	26.26±11.49	0.041±0.013	2.92(0.91)
Bulk Powder+ 13% Porogens	17.53±4.72	0.034±0.006	4.34(0.97)
Bulk Powder+ 16% Porogens	31.52±6.17	0.043±0.005	5.74(0.096)
Bulk Powder+ 25% Porogens	62.11±15.12	0.065±0.016	4.42(0.92)
Experiment 2 (Zb60)			
Bulk Powder	11.75±2.63	0.65±0.024	5.22(0.97)
Bulk Powder+ 10% Porogens	12.65±2.28	0.045±0.011	6.33(0.81)
Bulk Powder+ 20% Porogens	16.87±4.46	0.054±0.011	4.46(0.91)
Bulk Powder+ 25% Porogens	15.48±2.06	0.062±0.011	8.71(0.99)
Experiment 3			
(Zb60)Bulk Powder+ 20% Porogens	16.89±2.77	0.051±0.014	6.92(0.96)
Bulk Powder+ 20% Porogens	14.98±4.75	0.044±0.007	2.66(0.88)
Bulk Powder+ 25% Porogens	19.75±4.61	0.047±0.007	4.89(0.97)

Linear regression for the weibull modulus distribution used to predict the probability of failure of CPP part for all categories have been shown in Figure 12, Figure 13, and Figure 14 respectively for the Experiments 1-3, which were calculated using equations (6) and (7).

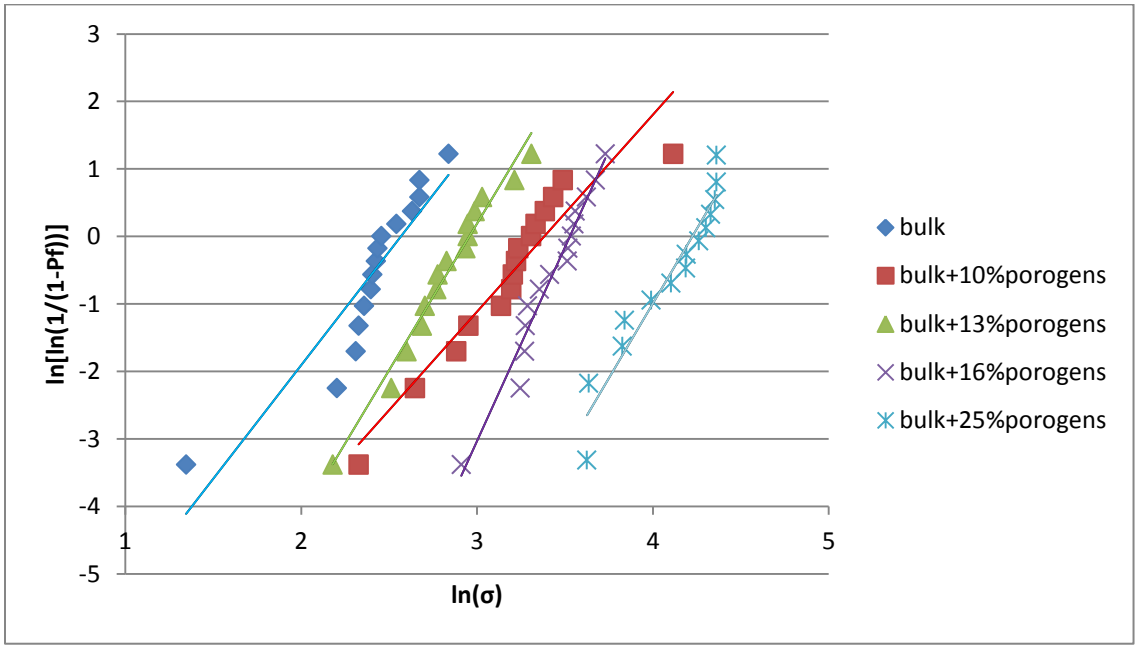

Figure 12. Weibull failure probability functions and linear interpolation for compressive strength of all categories within Experiment 1

In Experiment 1, shown in Figure 12, all the categories were fairly similar and close in weibull modulus values and the linear regression line patterns. In addition, by looking at the Table 7, it is almost clear that by increasing porogens percentage the weibull modulus value increases; so in Experiment 1 the category with 25% porogens ended up with the highest weibull modulus value. After looking at the results for Experiment 2, shown in Table 7 and Figure 13, similar patterns to Experiment 1 can be observed; however, the weibull modulus values were significantly improved in Experiment 2 compared to Experiment 1. The weibull

modulus and the linear regression lines for Experiment 3, shown in Table 7 and Figure 14, were very similar to the two previous experiments; if compared based on the liquid binder, the three categories in Experiment 3 followed the same behavior to the corresponding groups in the two previous experiments.

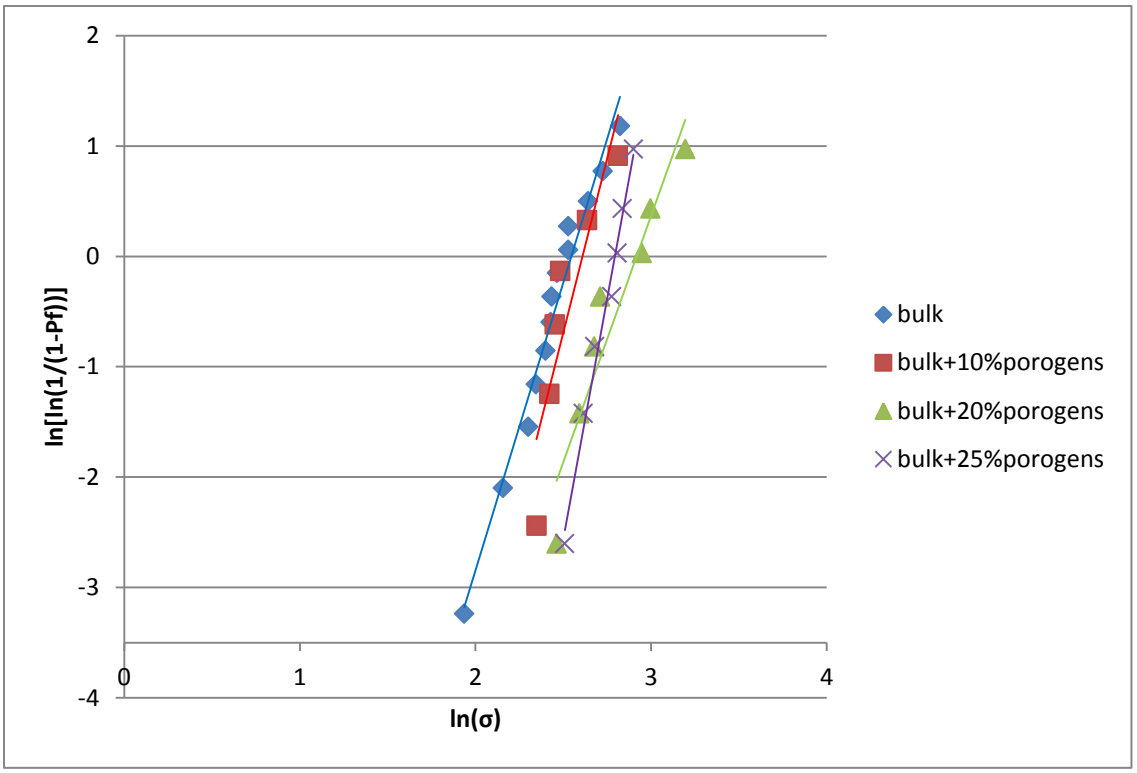

Figure 13. Weibull failure probability functions and linear interpolation for compressive strength of all categories within Experiment 2 (Zb60)

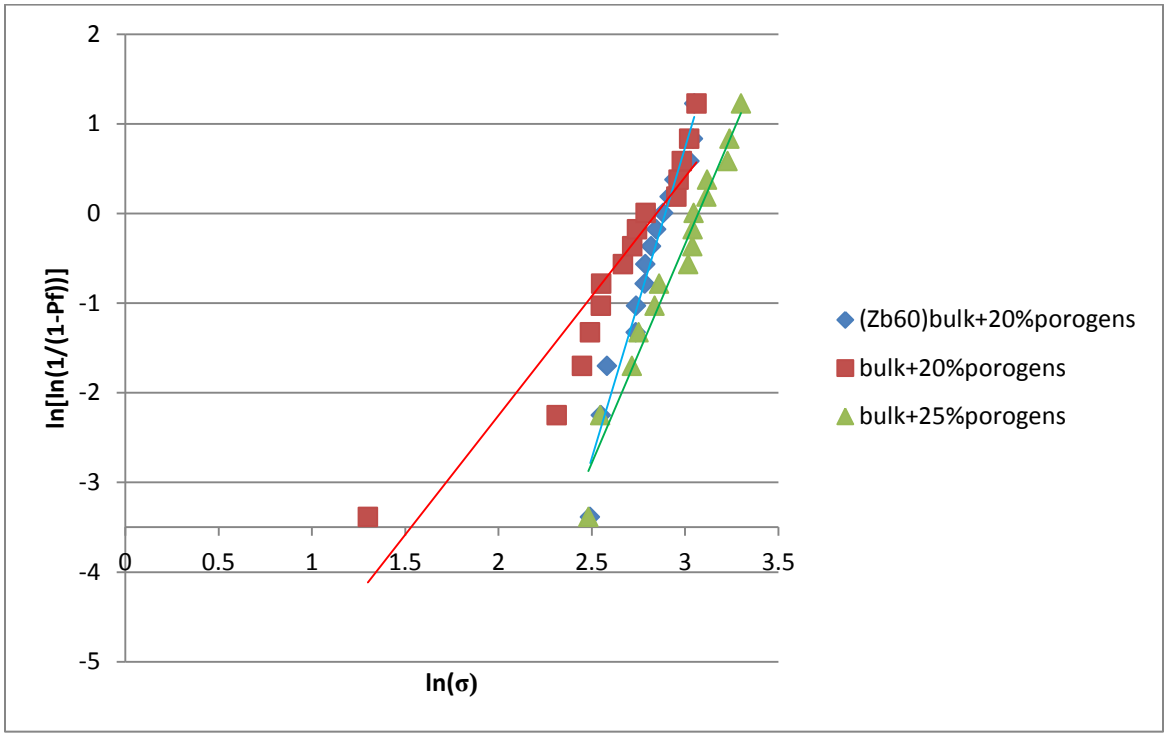

Figure 14. Weibull failure probability functions and linear interpolation for compressive strength of all categories within Experiment 3

4.1.5 Structural characterization: SEM Images

After examining the results obtained from all three experiments, Experiment 1 showed to be the most promising of them all. As a result it was decided to perform Scanning Electron Microscopy (SEM) on couple of samples from Experiment 1 for further structural analysis.

Samples were chosen randomly from different categories within Experiment 1 and as it was explained in the previous chapter, before SEM imaging all the samples had to be sputter-coated with a 10nm thick gold layer to be electrically conductive. There are 6 images in Figure 15 that were taken from two samples from categories with 16% and 25% porogens. Images a, b, and c were taken from a specimen with 25% porogens and the other three

images were taken from a sample with 16% porogens. The purpose of these images was to determine:

- If the particles have properly bonded with one another
- If the sinter necks were formed
- If the pores have been distributed uniformly throughout the part
- If the particle bindings resulted in a good surface of roughness

In Figure 15, Images c and f were taken with a lower magnification to have a better overall view of the parts. Image c is the side view of the cylindrical sample and image f is the top view. In both images c and d, it can be observed that the interconnected pores are evenly scattered throughout both parts. Images a, b, and e were taken with a higher magnification to see in microstructure of the parts more in details. The blue and red arrows in the images are examples showing, respectively, sinter necks and pores within the structure of the parts. It is quite clear in the images that the sinter necks and pores had been formed in various sizes. In Figure 15, image b, on the left side there is a large red arrow indicating a pore with a size of ~ 90 μm that was most likely created by the sacrificial porogens. Moreover, image d was taken with a higher magnification that indicated the surface roughness of the part and how smaller particles have bonded together.

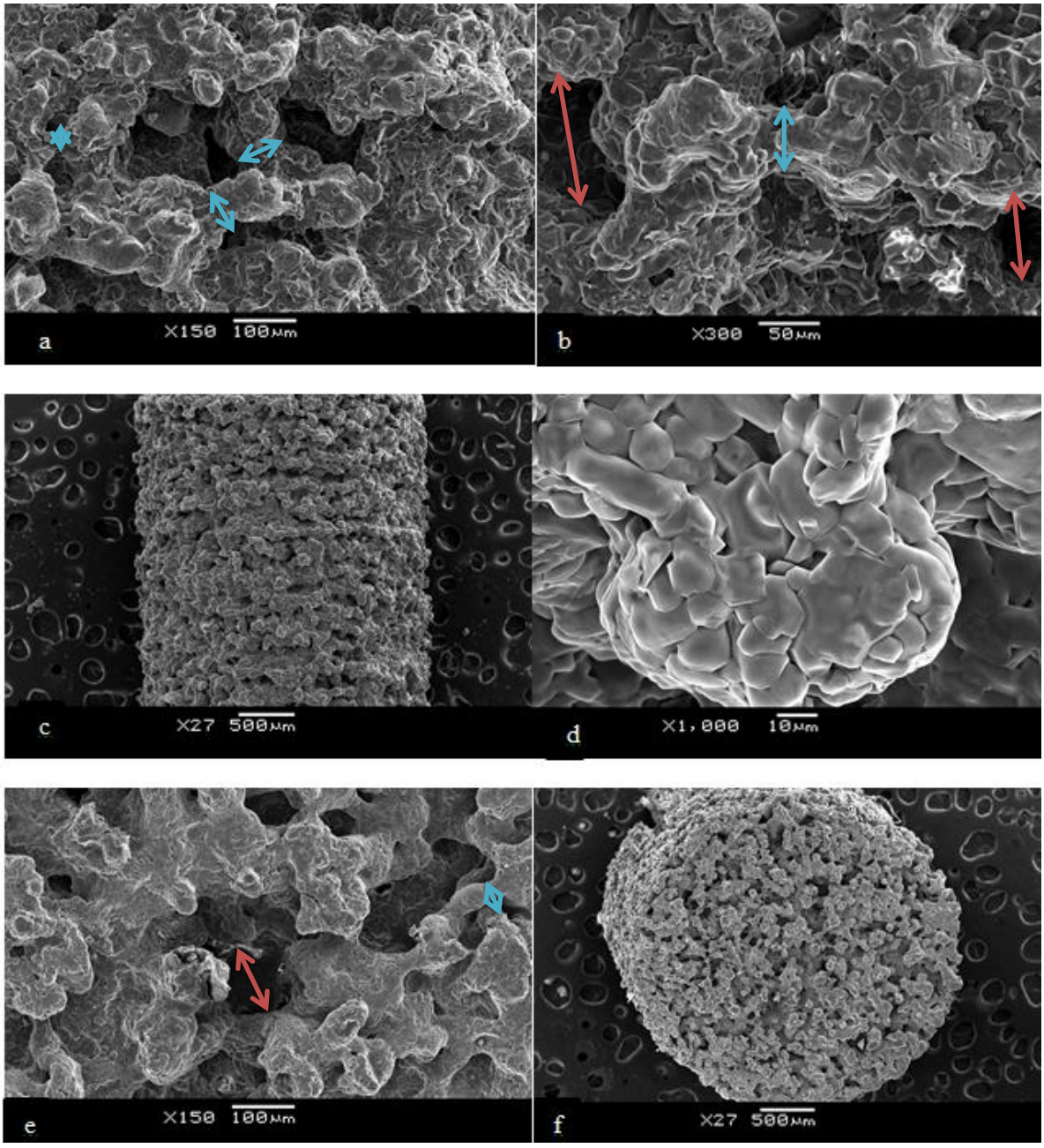

Figure 15. SEM images of sintered cylindrical CPP parts with various magnification levels; indicating the uniform porosity, surface roughness and interconnected pores. Images a, b, and c were taken from a sample which belonged to the category with 25% porogens in Experiment 1; and the other three images were taken from a specimen belonging to the category with 16% porogens in Experiment1

4.2 Discussion

Currently there is no exact application or use for fine CPP particles (<75µm) and most of the recent studies are based on using large particle CPP powder (75-150µm) [6, 20, 21, 24, 71]; the main achievement of this study is in representing the feasibility of using fine particle CPP powder for additive manufacturing and showing its potential.

The literature suggests that by using a finer particle size composition for powder based additive manufacturing flowability becomes more challenging [3, 26], it also proposes that a lower particle size could lead to improve mechanical properties by promoting sintering and intention for better packing density [3]. In the case of CPP powder, it was stablished that the large particle CPP (75-150 µm) powder has a good flow behavior; considering that, it was decided to mix porogens with the fine CPP powder. Porogens are sacrificial particles which are usually intended for creating additional pores in a structure, however in this case the porogens (PVA 75-106 µm) were intended for promoting better flowability. In the following, the results of three sets of experiment are discussed.

4.2.1 Experiment 1

In Experiment 1, the sintered part showed that as the percentage of porogens increases the porosity of the parts decreases; in Figure 11, the average porosity of the cylindrical parts with no porogens (bulk powder only) has been marked as 53.1% which is the highest value between other categories in Experiment 1. Following that, as the porogens percentage increases, the category with 25% porogens ended up having the lowest porosity with 38.7%. The decrease in porosity by increasing the porogens percentage suggests that the powder

flow behavior was improved and as a result spread more smoothly which led to a better layer compaction.

Vlasea et al. stablished that the shrinkage is greater when using the fine particle CPP [15]; and as it was expected the measured shrinkage shown in Table 6 for Experiment 1 was high. Furthermore as the percentage of porogens increases the shrinkage becomes more significant; increasing from 11.4%±4.2 (diameter) and 15.2%±2.9 (height) shrinkage with no porogens, to 27.8%±1.3 (diameter) and 28.1%±4.2 (height) with 25% porogens. Another observation, made by looking at the shrinkage measurements was that the shrinkage remained higher along the height of the samples than the diameter.

Uniaxial compression testing results were quite impressive. In Table 7, it can be seen that the bulk powder with no porogens had the lowest mechanical strength of 11.53±2.99 MPa and the powder with 25% porogens had the compressive strength of 62.11±15.12 MPa. In Figure 12, the Weibull failure probability functions and linear interpolation also shows some similar pattern between categories.

In summary, CPP parts with a porosity range from 38.7% to 53.1% were fabricated and demonstrated a compressive strength in the range of 11.53-62.11 MPa. Using the same 3D printing machine, the compressive strength reported by Shanjani et al. was in a range of 35-50 MPa which was based on using the large particle CPP (75-150 μm) as the main powder [9]; In the other word, the compressive strength results from Experiment 1 has met the previous findings and has improved them.

4.2.2 Experiment 2

Shortly after Experiment 1 it was found out that the liquid binder Zb58 is no longer at production, so instead Zb60 was purchased which was used as replacement for Zb58.

As a result, it was decided to repeat fabricating some of those categories in experiment 1, but this time with a slight change so the outcome could be an extended version of previous results. So by substituting two of previous powders the Experiment 2 had five categories including bulk powder, 10%, 20%, 25%, and 30% porogens mixed powder.

After the samples were fabricated and sintered, the shrinkage results showed that the increase in the porogens percentage leads to a higher shrinkage level. This behavior was expected after looking at the results of Experiment 1. By looking at the actual numbers this similarity gets more familiar; for example, the shrinkage for bulk powder in Experiment 1 and 2 were respectively 11.4%±4.2 (diameter), 15.2%±2.9 (height) and 12.8%±5.4 (diameter), 15.5%±3.7 (height). The limit to percentage of porogens is somewhere around 25%, because the sample that had 30% porogens had shrank significantly and by just looking at them, it seems that they were slightly melted which is not acceptable. In Figure 16, the sample on the left has 30% porogens; visually it is obvious that the one on the right side is almost twice as big. The samples with 30% porogens were not preceded with the rest of characterization process.

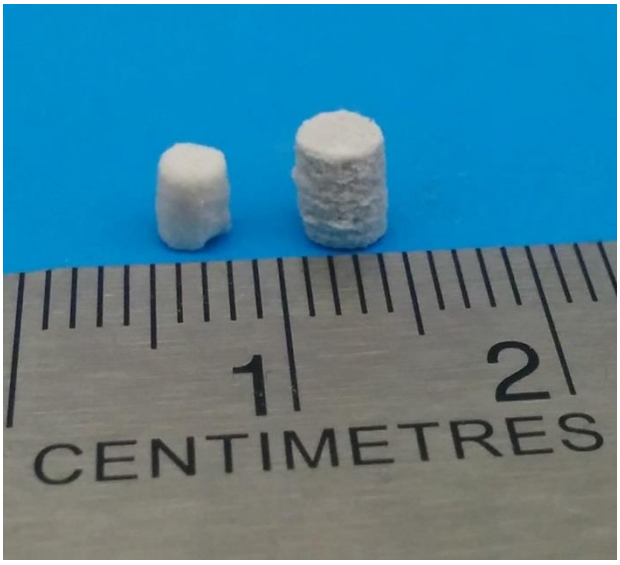

Figure 16. CPP cylindrical samples, the sample on the left has 30% porogens and the sample on the right has no porogens.

Unlike the shrinkage behavior, the porosity measurements were not exactly as predicted. The bulk powder with no porogens still has the highest porosity with 52.8%. However this time the drop in porosity percentage was not significant when the porogens percentage has been increased; at 25% porogens the porosity of 50.4% was achieved.

The compressive strength did not turn out to be as high as it was expected; however, the same pattern was observed which indicated that mixing additional porogens to the fine particle CPP powder improves mechanical strength. In Experiment 2, the bulk powder samples had a compressive strength equal to 11.75±2.63 MPa which is the only category that almost maintained the same strength in Experiment 1.

The considerably noted difference this time in Experiment 2 was that, the highest compressive strength was achieved by the samples with 20% porogens and it was only 16.87±4.46 MPa. The only thing that was significantly improved in Experiment 2 was the

standard deviation and the Weibull modulus which can be easily spotted in the Table 7 and Figure 13.

Looking back at the results obtain from the second experiment, some of the obtained CPP structures could fit the criteria for cancellous bone applications which requires a porosity range of 50-90% and a mechanical strength between 4 to 12MPa [72, 75].

4.2.3 Experiment 3

Going through the results for first two experiments, the changes were quite noticeable and nothing was altered along the additive manufacturing process or the characterization procedure, except the liquid binder; Zb58 was used for Experiment 1 and Zb60 for Experiment 2.

According to the outcome of both experiments, it is obvious that Zb58 has proven to be a better binder with outstanding results. The distributer company for Zb58 was contacted and a request was made for a new batch of Zb58 to be made.

After receiving the new Zb58 liquid binder it was decided to repeat manufacturing the cylindrical CPP structures for two categories including 20% and 25% porogens mixed powders. Moreover the batch with 20% porogens was used twice, once with Zb60 and then Zb58. Experiment 3 ended up having three categories including 20%, 25% porogens (Zb58), and 20% porogens (Zb60).

This time the shrinkage results were rather consistent and very close to what was predicted. In the case of Zb58, by increasing the porogens percentage from 20% to 25%, the shrinkage was increased slightly. Comparing the categories with 20% porogens, the one

made with Zb60 had slightly lower shrinkage percentage compare to the one made with Zb58 liquid binder.

As for porosity, the two categories with 20% porogens have porosities of 47.49% and 47.23% respectively for Zb60 and Zb58. And by increasing the porogens from 20% to 25%, the porosity was decreased. The group with 25% porogens had a porosity of 45.89% which was not as low as 38% achieved in the Experiment 1, but it had been decrease by ~ 5% from 50.39% that was achieved using Zb60 in the Experiment 2.

The uniaxial compression test results suggested that the sample group with 20% porogens which was 3D printed by dispersing Zb60 as the liquid binder, had a better consistency. The samples with 20% porogens (Zb60) have a mechanical strength of 16.89±2.77 MPa and that is almost identical to the value was obtained in Experiment 2 which was 16.87±4.46 MPa. As for the other two groups that were made using Zb58 liquid binder, the compressive strength was increased from 14.98±4.75 MPa to 19.75±4.61 MPa when porogens percentage added increased from 20% to 25%.

4.2.4 Mutual Trend in Three Experiments

Even though all of the experiments outcomes were different in terms of numbers, the behavior and the way those numbers changed were very alike. These patterns are including:

- The shrinkage was more significant when the porogens percentage was higher.
- The porosity percentage slightly dropped every time more porogens were added.
- The mechanical strength was improved by adding porogens.

All these statements mean that the large sacrificial particles (Porogens) had a positive impact on the fine particle CPP (< 75 μm) powder in which it intend to be the improvement in the flowability. Furthermore, these results indicated that the liquid binder has a significant effect on the properties of the CPP structures. Moreover, the differences in the results obtain from Experiment 1 and Experiment 3 suggests that the integrity of the new Zb58 that was obtained for the last experiment could be questionable.

One other observation after sintering was that after the cylindrical CPP structures were sintered, the color of parts were slightly changed to gray; same thing was observed for all experiments. This anomaly was reported previously by Vlasae et al. [15], saying that this is most likely due to the fact that the sintering protocols are mainly based on the large particle CPP powder.

First experiment proved to have the best results out of the other experiments. For further clarification of the structural characteristics, the scanning electron microscopy (SEM) images were obtained and analyzed from one or two samples that were chosen randomly from two different categories in Experiment 1. In Figure 15, the images a, b, and c were obtain from a sample that was selected from the group with 25% porogens; and the images d, e, and f were taken from a specimen that was chosen from the category with 16 % porogens. In all SEM images it is clear that the interconnected pores have been distributed uniformly and randomly in all regions. Image d in the Figure 15, shows the magnified view of a particle surface roughness. In Figure 15, there are pore that have been marked by red arrows which had a size range of 50-86 μm; the pores larger than 75 μm were created most likely by the

porogens (the large sacrificial particles). Furthermore, the sinter necks were well connected and some of them have been marked with a blue marker ranging from 30 to 50 µm.

4.2.5 Powder Analysis

The report that was sent back from ATS Scientific laboratory was analyzed and it showed that after all the hypothesis that the porogens are improving the flowability of the powder, is a fact. The report includes many different aspects of the powders which can be found in appendix 2; it has been shown in the Figure 10 that the flowability energy increases when porogens are added. By looking at Figure 10, it is clear that the pink line which presents the large particle CPP powder (75-150 µm) has the best flowability; and the green line presenting the fine particle CPP powder (< 75 µm) has the lowest flowability energy. The blue line presents the fine powder CPP with 25% porogens added, and clearly has a higher flowability energy trend that proves porogens are improving the flow behavior in the fine powder significantly.

Additionally, the powder particle size analysis obtained from the laser diffraction machine states that the average particle size for the fine CPP powder has a range of 41.27-42.76 µm (Table 5); and this value is almost 1/3 of the average obtained from large particle CPP powder which is 110.14 µm.

4.2.6 The Impact on Previous Findings

Table 8 describes a comparison between the results obtained from the current study and the previous findings related to additive manufacturing CPP done by Shanjani et al. and

Vlasea et al. [9, 15, 71]. The sintering protocol and the part geometry (cylindrical shaped: 4mm in diameter and 6mm in height) were the same for all three studies; the current study and the one done by Shanjani et al. both used same AM system (Zprinter 310plus), however, Vlasea et al. mainly used a different AM system [9, 15].

The bulk porosity achieved in the current study using the fine particle CPP powder covers almost both porosity ranges obtained by Shanjani et al. and Vlasea et al. The shrinkage percentage for the current study was higher than the values mentioned in the previous investigations but this increase in shrinkage was not surprising because Vlasea et al. also mentioned an increase in shrinkage when the fine particle CPP powder was used. The higher shrinkage percentage in this study could have been caused by simply adding the large particle sacrificial porogens to the powder mixture. Additionally, the highest shrinkage percentage in the current study was ~ 34% which was corresponding to the category with 30% porogens added to their powder mixture, but it was not mentioned in Table 8 because the resulted parts were not acceptable.

The compressive strength values obtained in this study have repeated almost all of those previous finding that were achieved by Shanjani et al. and Vlasea et al. The maximum average compressive strength, that was achieved before, was ~ 50 MPa which was done by Shanjani et al. using the large particle CPP powder and Zb58 as the liquid binder [9] and in the current investigation, the maximum average compressive strength has been recorded as ~ 62 MPa which was obtained by using the fine particle CPP powder and Zb58 as the liquid binder. The corresponding category to 62 MPa had 25% porogens mixed with the fine CPP powder. According to these results, additive manufacturing samples using fine particle CPP

powder with 25% porogens instead of large particle CPP powder, can lead to specimens with improved mechanical properties.

After examining the results achieved in this investigation and comparing them with the previous findings that were done by Shanjani et al. and Vlasea et al., evidences are indicating a great potential for use of fine particle CPP powder as a replacement to large particle CPP powder.

Table 8. Comparison between current and previous finding related to additive manufacturing of CPP powder [9, 15, 71]

	Shanjani et al.	**Vlasea et al.**	**Current Study**
CPP Powder Particle Size (µm)	75-150	75-150, < 75	< 75
Liquid Binder	Zb58	Zb58	Zb58, Zb60
Bulk Porosity (%)	~ 35-38	~ 30-55	~ 39-53
Compressive Strength (MPa)	~ 34-50	~ 2.9-45	~ 11-62
Dimensional Shrinkage (%)	~ 12-18	~ 10-20	~ 11-28

4.3 Summary

More than 165 samples were made for this thesis and 152 of which were sintered and characterized accordingly. In this study, by altering the porogens percentage between 0, 10, 13, 16, 20, and 25% and mixing them with the fine CPP bulk powder, within statistical significant, the resulting bulk porosity of additive manufactured cylindrical structures changed between 38.67-53.07% while the compressive strength set to be a rage of 11.5-62.1 MPa. The results stated that by adding porogens to the fine powder, a better flow performance can be attained. The powder flowability testing results using FT4 Rheometer also supported the same hypothesis that by adding larger particles it can improve the flowability of a finer powder.

Chapter 5
Conclusions and Future work

5.1 Conclusion

The main purpose of this work which is to 3D print cylindrical CPP parts using the fine powder (CPP < 75 µm) was established. This thesis presented a novel method to solve the flowability issue when using a fine particle size powder within the 3D printing process.

The proposed solution was very simple; an additional percentage of a large particle sacrificial powder (porogens) had to be mixed with the default fine powder to promote better flow behavior in order to be spread smoothly. In the case of CPP powder, it was suggested that the size of the porogens particles should be something in the range of 75-150 µm which is the size of the large particle CPP powder. As a result PVA 75-106 µm was chosen to be the large particle sacrificial powder.

Experiment 1 was the first approach which had 5 different groups of samples. These groups differentiate from each other based on their powders which included bulk powder, bulk+10% porogens powder, bulk+13% porogens, bulk+16% porogens, and bulk+25% porogens. A Layer thickness of 125µm and the liquid binder Zb58 was used to fabricate all of the samples within those five categories.74 samples in total were sintered and characterized; within statistical significant, a porosity range of 38.7-53.1% was achieved with a compressive strength ranging from 11.52 MPa to 62.11 MPa.

Experiment 2 was the second approach which had four categories including bulk powder, bulk+10% porogens powder, bulk+20% porogens, and bulk+25% porogens. This time Zb60 was used as the liquid binder instead of Zb58 and the layer thickness remained the same (125 µm).33 samples were sintered and characterized; the porosity of the CPP samples were determined ranging from 49.3% to 52.8% with a compressive strength of 11.7-16.9 MPa.

The last attempt was Experiment 3 which had three categories. Fist category which was bulk+20% porogens was 3D printed using Zb60 as the liquid binder. And the other two categories, bulk+20% porogens and bulk+25% porogens were fabricated using a new batch of Zb58. The layer thickness stayed the same as the other two experiments. The total of 45 sintered samples went through the characterization process; the samples that were fabricated using the Zb60 binder ended up with a porosity of 47.5% corresponding with a compressive strength of 16.9 MPa. Following that, the samples that were manufactured using the new Zb58 binder, bulk+20% porogens and bulk+25% porogens, respectively had a porosity of 47.2% and 45.9% with a compressive strength equal to 14.9 MPa and 19.8 MPa.

In conclusion, this thesis has proven 3D printing fine CPP powder is feasible and can be improved by new means. Additionally, the results that were archived previously by Shanjani et al. using large particle CPP powder (75-150 µm) and layer thicknesses including 150 µm and 175 µm, can be recreated and improved using fine CPP powder (<75 µm) and a layer thickness of 125 µm. Furthermore, the results provided in this work suggested that the structures made from the fine CPP powder fit the requirements for the cancellous bone applications.

5.2 Future work

Based on the results that were achieved in this study, it is recommended for future further investigation:

- Getting two diverse set of results from using two different batch of same binder (Zb58) suggested that finding and changing the liquid binder can lead to a better process optimization and more consistent results.
- There is no optimize heat treatment protocol specifically designed for fine CPP powder, and finding a better sintering protocol can lead to a better final product with improved mechanical properties.
- A larger particle size porogens substrate with a particle size of 106-125 μm and a more sphere-shaped form can result in a better flow behavior.
- A narrower range of particle size could also lead to a better consistent set of results with better mechanical properties, for example CPP with a particle size of 40-75 μm.
- Investigating an alternative material choice instead of PVA as the porogens substrate, could result in a better microstructure and ultimately.

References

[1] A. A. White, S. M. Best, and I. A. Kinloch, "Hydroxyapatite–Carbon Nanotube Composites for Biomedical Applications: A Review," *Int. J. Appl. Ceram. Technol.*, vol. 4, no. 1, pp. 1–13, 2007.

[2] K. A. Hing, "Bioceramic Bone Graft Substitutes: Influence of Porosity and Chemistry," *Int. J. Appl. Ceram. Technol.*, vol. 2, no. 3, pp. 184–199, 2005.

[3] J. Will, R. Melcher, C. Treul, N. Travitzky, U. Kneser, E. Polykandriotis, R. Horch, and P. Greil, "Porous ceramic bone scaffolds for vascularized bone tissue regeneration," *J. Mater. Sci. Mater. Med.*, vol. 19, no. 8, pp. 2781–2790, Aug. 2008.

[4] D. W. Hutmacher, "Scaffolds in tissue engineering bone and cartilage," *Biomaterials*, vol. 21, no. 24, pp. 2529–2543, Dec. 2000.

[5] D. Baksh, J. E. Davies, and S. Kim, "Three-dimensional matrices of calcium polyphosphates support bone growth in vitro and in vivo," *J. Mater. Sci. Mater. Med.*, vol. 9, no. 12, pp. 743–748, Dec. 1998.

[6] Y. Shanjani, J. N. A. De Croos, R. M. Pilliar, R. A. Kandel, and E. Toyserkani, "Solid freeform fabrication and characterization of porous calcium polyphosphate structures for tissue engineering purposes," *J. Biomed. Mater. Res. B Appl. Biomater.*, vol. 93B, no. 2, pp. 510–519, May 2010.

[7] R. A. Kandel, M. Grynpas, R. Pilliar, J. Lee, J. Wang, S. Waldman, P. Zalzal, and M. Hurtig, "Repair of osteochondral defects with biphasic cartilage-calcium polyphosphate constructs in a Sheep model," *Biomaterials*, vol. 27, no. 22, pp. 4120–4131, Aug. 2006.

[8] M. D. Grynpas, R. M. Pilliar, R. A. Kandel, R. Renlund, M. Filiaggi, and M. Dumitriu, "Porous calcium polyphosphate scaffolds for bone substitute applications in vivo studies," *Biomaterials*, vol. 23, no. 9, pp. 2063–2070, May 2002.

[9] Y. Shanjani, "Solid Freeform Fabrication of Porous Calcium Polyphosphate Structures for Use in Orthopaedics," Sep. 2011.

[10] T. Vasilopoulos, "High Productivity Milling of Calcium Polyphosphate."

[11] Y. Shanjani, E. Toyserkani, and C. Wei, "Modeling and Characterization of Biomaterials Spreading Properties in Powder-Based Rapid Prototyping Techniques," pp. 135–143, Jan. 2007.

[12] R. M. Pilliar, J. Hong, and J. P. Santerre, *Method of manufacture of porous inorganic structures*. Google Patents, 2009.

[13] R. M. Pilliar, M. J. Filiaggi, J. D. Wells, M. D. Grynpas, and R. A. Kandel, "Porous calcium polyphosphate scaffolds for bone substitute applications — in vitro characterization," *Biomaterials*, vol. 22, no. 9, pp. 963–972, May 2001.

[14] N. L. Porter, R. M. Pilliar, and M. D. Grynpas, "Fabrication of porous calcium polyphosphate implants by solid freeform fabrication: A study of processing parameters and in vitro degradation characteristics," *J. Biomed. Mater. Res.*, vol. 56, no. 4, pp. 504–515, Sep. 2001.

[15] M. Vlasea, "Additive Manufacturing Methodology and System for Fabrication of Porous Structures with Functionally Graded Properties," Feb. 2014.

[16] K. F. Leong, C. M. Cheah, and C. K. Chua, "Solid freeform fabrication of three-dimensional scaffolds for engineering replacement tissues and organs," *Biomaterials*, vol. 24, no. 13, pp. 2363–2378, Jun. 2003.

[17] J. Suwanprateeb and R. Chumnanklang, "Three-dimensional printing of porous polyethylene structure using water-based binders," *J. Biomed. Mater. Res. B Appl. Biomater.*, vol. 78B, no. 1, pp. 138–145, Jul. 2006.

[18] A. Basalah, Y. Shanjani, S. Esmaeili, and E. Toyserkani, “Characterizations of additive manufactured porous titanium implants,” *J. Biomed. Mater. Res. B Appl. Biomater.*, vol. 100B, no. 7, pp. 1970–1979, 2012.
[19] M. Vlasea, Y. Shanjani, A. Bothe, R. Kandel, and E. Toyserkani, “A combined additive manufacturing and micro-syringe deposition technique for realization of bio-ceramic structures with micro-scale channels,” *Int. J. Adv. Manuf. Technol.*, vol. 68, no. 9–12, pp. 2261–2269, Oct. 2013.
[20] Y. Shanjani, Y. Hu, E. Toyserkani, M. Grynpas, R. A. Kandel, and R. M. Pilliar, “Solid freeform fabrication of porous calcium polyphosphate structures for bone substitute applications: In vivo studies,” *J. Biomed. Mater. Res. B Appl. Biomater.*, vol. 101B, no. 6, pp. 972–980, 2013.
[21] M. Vlasea, E. Toyserkani, and R. Pilliar, “Effect of Gray Scale Binder Levels on Additive Manufacturing of Porous Scaffolds with Heterogeneous Properties,” *Int. J. Appl. Ceram. Technol.*, vol. 12, no. 1, pp. 62–70, Jan. 2015.
[22] S. D. Waldman, M. D. Grynpas, R. M. Pilliar, and R. A. Kandel, “Characterization of cartilagenous tissue formed on calcium polyphosphate substrates in vitro,” *J. Biomed. Mater. Res.*, vol. 62, no. 3, pp. 323–330, 2002.
[23] Y. Hu, Y. Shanjani, E. Toyserkani, M. Grynpas, R. Wang, and R. Pilliar, “Porous calcium polyphosphate bone substitutes: Additive manufacturing versus conventional gravity sinter processing—Effect on structure and mechanical properties,” *J. Biomed. Mater. Res. B Appl. Biomater.*, vol. 102, no. 2, pp. 274–283, 2014.
[24] M. Vlasea and E. Toyserkani, “Experimental characterization and numerical modeling of a micro-syringe deposition system for dispensing sacrificial photopolymers on particulate ceramic substrates,” *J. Mater. Process. Technol.*, vol. 213, no. 11, pp. 1970–1977, Nov. 2013.
[25] R. Freeman, “Measuring the flow properties of consolidated, conditioned and aerated powders — A comparative study using a powder rheometer and a rotational shear cell,” *Powder Technol.*, vol. 174, no. 1–2, pp. 25–33, May 2007.
[26] I. Gibson, D. W. Rosen, and B. Stucker, *Additive Manufacturing Technologies*. Boston, MA: Springer US, 2010.
[27] Y. Ikada and H. Tsuji, “Biodegradable polyesters for medical and ecological applications,” *Macromol. Rapid Commun.*, vol. 21, no. 3, pp. 117–132, 2000.
[28] L. E. Claes, “Mechanical characterization of biodegradable implants,” *Clin. Mater.*, vol. 10, no. 1–2, pp. 41–46, 1992.
[29] P. Rokkanen, S. Vainionpää, P. Törmälä, J. Kilpikari, O. Böstman, K. Vihtonen, J. Laiho, and M. Tamminmäki, “BIODEGRADABLE IMPLANTS IN FRACTURE FIXATION: EARLY RESULTS OF TREATMENT OF FRACTURES OF THE ANKLE,” *The Lancet*, vol. 325, no. 8443, pp. 1422–1424, Jun. 1985.
[30] L. L. Hench, “Bioceramics: From Concept to Clinic,” *J. Am. Ceram. Soc.*, vol. 74, no. 7, pp. 1487–1510, Jul. 1991.
[31] W. R. Moore, S. E. Graves, and G. I. Bain, “Synthetic bone graft substitutes,” *ANZ J. Surg.*, vol. 71, no. 6, pp. 354–361, Jun. 2001.
[32] A. K. Mohanty, M. Misra, and G. Hinrichsen, “Biofibres, biodegradable polymers and biocomposites: An overview,” *Macromol. Mater. Eng.*, vol. 276–277, no. 1, pp. 1–24, Mar. 2000.
[33] J. L. Ong, M. R. Appleford, and G. Mani, *Introduction to Biomaterials: Basic Theory with Engineering Applications*. Cambridge University Press, 2013.
[34] B. D. Ratner, *Biomaterials Science: An Introduction to Materials in Medicine*. Academic Press, 2004.
[35] J. P. Bilezikian, L. G. Raisz, and T. J. Martin, *Principles of Bone Biology: Two-Volume Set*. Academic Press, 2008.

[36] D. W. Hutmacher, J. T. Schantz, C. X. F. Lam, K. C. Tan, and T. C. Lim, "State of the art and future directions of scaffold-based bone engineering from a biomaterials perspective," *J. Tissue Eng. Regen. Med.*, vol. 1, no. 4, pp. 245–260, 2007.
[37] B. D. Ratner, *Biomaterials science an introduction to materials in medicine*. [Place of publication not identified]: Academic Press, 2013.
[38] H. Yuan, K. Kurashina, J. D. de Bruijn, Y. Li, K. de Groot, and X. Zhang, "A preliminary study on osteoinduction of two kinds of calcium phosphate ceramics," *Biomaterials*, vol. 20, no. 19, pp. 1799–1806, Oct. 1999.
[39] T. Kitsugi, T. Yamamuro, T. Nakamura, S. Kotani, T. Kokubo, and H. Takeuchi, "Four calcium phosphate ceramics as bone substitutes for non-weight-bearing," *Biomaterials*, vol. 14, no. 3, pp. 216–224, 1993.
[40] P. Frayssinet, J. L. Trouillet, N. Rouquet, E. Azimus, and A. Autefage, "Osseointegration of macroporous calcium phosphate ceramics having a different chemical composition," *Biomaterials*, vol. 14, no. 6, pp. 423–429, May 1993.
[41] T.-M. G. Chu, D. G. Orton, S. J. Hollister, S. E. Feinberg, and J. W. Halloran, "Mechanical and in vivo performance of hydroxyapatite implants with controlled architectures," *Biomaterials*, vol. 23, no. 5, pp. 1283–1293, Mar. 2002.
[42] T. Dutta Roy, J. L. Simon, J. L. Ricci, E. D. Rekow, V. P. Thompson, and J. R. Parsons, "Performance of hydroxyapatite bone repair scaffolds created via three-dimensional fabrication techniques," *J. Biomed. Mater. Res. A*, vol. 67A, no. 4, pp. 1228–1237, Dec. 2003.
[43] B. Rw, C. A, and H. Re, "Hydroxyapatite and tricalcium phosphate bone graft substitutes.," *Orthop. Clin. North Am.*, vol. 18, no. 2, pp. 323–334, Apr. 1987.
[44] M. Ds, D. Td, and P. Jr, "Tricalcium phosphate ceramic--a resorbable bone implant: review and current status.," *J. Am. Dent. Assoc. 1939*, vol. 105, no. 6, pp. 1035–1038, Dec. 1982.
[45] L. G. Zhang, J. P. Fisher, and Leung, *Additive manufacturing for bone load bearing applications*. Elsevier, 2015.
[46] C.-H. Wei, "Rapid Fabrication Techniques for Anatomically-Shaped Calcium Polyphosphate Substrates for Implants to Repair Osteochondral Focal Defects," University of Waterloo, 2007.
[47] R. M. Pilliar, R. A. Kandel, M. D. Grynpas, P. Zalzal, and M. Hurtig, "Osteochondral defect repair using a novel tissue engineering approach: Sheep model study," *Technol. Health Care*, vol. 15, no. 1, pp. 47–56, Jan. 2007.
[48] S. R. Nelson, L. M. Wolford, R. J. Lagow, P. J. Capano, and W. L. Davis, "Evaluation of new high-performance calcium polyphosphate bioceramics as bone graft materials," *J. Oral Maxillofac. Surg.*, vol. 51, no. 12, pp. 1363–1371, Dec. 1993.
[49] R. Huang and R. N. Reusch, "Genetic competence in Escherichia coli requires poly-beta-hydroxybutyrate/calcium polyphosphate membrane complexes and certain divalent cations.," *J. Bacteriol.*, vol. 177, no. 2, pp. 486–490, Jan. 1995.
[50] K. Qiu, C. X. Wang, Q. Zhang, X. Chen, and H. Su, "In Vitro Degradation Studies of Calcium Polyphosphate Ceramics Prepared by Controlled Degree of Polymerization and Crystallization," *Key Eng. Mater.*, vol. 288–289, pp. 553–556, 2005.
[51] K. Qiu, C. X. Wan, C. S. Zhao, X. Chen, C. W. Tang, and Y. W. Chen, "Fabrication and characterization of porous calcium polyphosphate scaffolds," *J. Mater. Sci.*, vol. 41, no. 8, pp. 2429–2434, Apr. 2006.
[52] C. K. Chua, K. F. Leong, and C. S. Lim, *Rapid Prototyping: Principles and Applications*. World Scientific, 2010.
[53] J.-P. Kruth, M. C. Leu, and T. Nakagawa, "Progress in Additive Manufacturing and Rapid Prototyping," *CIRP Ann. - Manuf. Technol.*, vol. 47, no. 2, pp. 525–540, 1998.

[54] B. C. Gross, J. L. Erkal, S. Y. Lockwood, C. Chen, and D. M. Spence, "Evaluation of 3D Printing and Its Potential Impact on Biotechnology and the Chemical Sciences," *Anal. Chem.*, vol. 86, no. 7, pp. 3240–3253, Apr. 2014.
[55] F. P. W. Melchels, M. A. N. Domingos, T. J. Klein, J. Malda, P. J. Bartolo, and D. W. Hutmacher, "Additive manufacturing of tissues and organs," *Prog. Polym. Sci.*, vol. 37, no. 8, pp. 1079–1104, Aug. 2012.
[56] J. Bredt, A. C. M. E. T. Fan, K. S. Lee, B. Pruitt, and P. Williams, "Dimensional Printing: Rapid Tooling and Prototypes Directly from CAD Representation."
[57] A. Butscher, M. Bohner, S. Hofmann, L. Gauckler, and R. Müller, "Structural and material approaches to bone tissue engineering in powder-based three-dimensional printing," *Acta Biomater.*, vol. 7, no. 3, pp. 907–920, Mar. 2011.
[58] H. L. Yoo J, Cima MJ, Khanuja S, Sachs EM, "Structural ceramic components by 3D printing," Solid freeform fabrication symposium, Austin, TX, 1993.
[59] R. A. Giordano, B. M. Wu, S. W. Borland, L. G. Cima, E. M. Sachs, and M. J. Cima, "Mechanical properties of dense polylactic acid structures fabricated by three dimensional printing," *J. Biomater. Sci. Polym. Ed.*, vol. 8, no. 1, pp. 63–75, Jan. 1997.
[60] R. Chumnanklang, T. Panyathanmaporn, K. Sitthiseripratip, and J. Suwanprateeb, "3D printing of hydroxyapatite: Effect of binder concentration in pre-coated particle on part strength," *Mater. Sci. Eng. C*, vol. 27, no. 4, pp. 914–921, May 2007.
[61] A. Khalyfa, S. Vogt, J. Weisser, G. Grimm, A. Rechtenbach, W. Meyer, and M. Schnabelrauch, "Development of a new calcium phosphate powder-binder system for the 3D printing of patient specific implants," *J. Mater. Sci. Mater. Med.*, vol. 18, no. 5, pp. 909–916, May 2007.
[62] U. Gbureck, T. Hölzel, C. J. Doillon, F. A. Müller, and J. E. Barralet, "Direct Printing of Bioceramic Implants with Spatially Localized Angiogenic Factors," *Adv. Mater.*, vol. 19, no. 6, pp. 795–800, Mar. 2007.
[63] U. Gbureck, E. Vorndran, F. A. Müller, and J. E. Barralet, "Low temperature direct 3D printed bioceramics and biocomposites as drug release matrices," *J. Controlled Release*, vol. 122, no. 2, pp. 173–180, Sep. 2007.
[64] J. Suwanprateeb, R. Sanngam, W. Suvannapruk, and T. Panyathanmaporn, "Mechanical and in vitro performance of apatite–wollastonite glass ceramic reinforced hydroxyapatite composite fabricated by 3D-printing," *J. Mater. Sci. Mater. Med.*, vol. 20, no. 6, pp. 1281–1289, Jun. 2009.
[65] U. Gbureck, T. Hölzel, I. Biermann, J. E. Barralet, and L. M. Grover, "Preparation of tricalcium phosphate/calcium pyrophosphate structures via rapid prototyping," *J. Mater. Sci. Mater. Med.*, vol. 19, no. 4, pp. 1559–1563, Apr. 2008.
[66] C. X. F. Lam, X. M. Mo, S. H. Teoh, and D. W. Hutmacher, "Scaffold development using 3D printing with a starch-based polymer," *Mater. Sci. Eng. C*, vol. 20, no. 1–2, pp. 49–56, May 2002.
[67] B. M. Wu, S. W. Borland, R. A. Giordano, L. G. Cima, E. M. Sachs, and M. J. Cima, "Solid free-form fabrication of drug delivery devices," *J. Controlled Release*, vol. 40, no. 1–2, pp. 77–87, Jun. 1996.
[68] K. Igawa, M. Mochizuki, O. Sugimori, K. Shimizu, K. Yamazawa, H. Kawaguchi, K. Nakamura, T. Takato, R. Nishimura, S. Suzuki, M. Anzai, U. Chung, and N. Sasaki, "Tailor-made tricalcium phosphate bone implant directly fabricated by a three-dimensional ink-jet printer," *J. Artif. Organs*, vol. 9, no. 4, pp. 234–240, Dec. 2006.
[69] W. Sun, "Bio-CAD modeling and its applications in computer-aided tissue engineering," *Comput.-Aided Des.*, vol. 37, no. 11, pp. 1097–1114.

[70] D. W. Hutmacher, M. Sittinger, and M. V. Risbud, "Scaffold-based tissue engineering: rationale for computer-aided design and solid free-form fabrication systems," *Trends Biotechnol.*, vol. 22, no. 7, pp. 354–362, Jul. 2004.
[71] Y. Shanjani, Y. Hu, R. M. Pilliar, and E. Toyserkani, "Mechanical characteristics of solid-freeform-fabricated porous calcium polyphosphate structures with oriented stacked layers," *Acta Biomater.*, vol. 7, no. 4, pp. 1788–1796, Apr. 2011.
[72] V. Karageorgiou and D. Kaplan, "Porosity of 3D biomaterial scaffolds and osteogenesis," *Biomaterials*, vol. 26, no. 27, pp. 5474–5491, Sep. 2005.
[73] A. Khalili and K. Kromp, "Statistical properties of Weibull estimators," *J. Mater. Sci.*, vol. 26, no. 24, pp. 6741–6752, Dec. 1991.
[74] D. Wu, J. Zhou, and Y. Li, "Methods for estimating Weibull parameters for brittle materials," *J. Mater. Sci.*, vol. 41, no. 17, pp. 5630–5638, Sep. 2006.
[75] S. Yang, K.-F. Leong, Z. Du, and C.-K. Chua, "The Design of Scaffolds for Use in Tissue Engineering. Part I. Traditional Factors," *Tissue Eng.*, vol. 7, no. 6, pp. 679–689, Dec. 2001.

Appendix A

Dynamic Measurements Done by ATS Scientific Laboratory

- Powder1: Bulk powder (90% CPP < 75µm+10% PVA < 63 µm)
- Powder 2: Bulk powder +25% Porogens
- Powder 3: Large particle bulk powder (90% CPP 75-150+10% PVA < 63 µm)

Table A-1. The results determined by using the different methodologies of the FT4

Dynamic Measurements	Powder 1	Powder 2	Powder 3
Basic Flowability Energy, BFE (mJ)	115	159	291
Stability Index, SI	0.856	0.817	0.958
Flow Rate Index, FRI	1.49	1.32	1.04
Specific Energy, SE (mJ/g)	5.05	5.40	3.99
Conditioned Bulk Density, CBD (g/ml)	0.693	0.770	1.16
Aeration Ratio, AR10mm/s	21.9	6.84	6.18
Aerated Energy, AE10mm/s (mJ)	6.01	26.0	50.3
Normalized Aeration Sensitivity, NAS (s/mm)	0.280	0.314	0.130

The definition of each parameter measured in the Table A-1 has been given in the Table A-2.

Table A-2. The definition of parameters measured by different methodologies of the FT4

Measurement:	Definition:
Basic Flowability Energy	The energy needed to displace a conditioned and stabilized powder at a given flow pattern and flow rate – in this investigation at -5° helix and 100mm/s blade tip speed and a sample volume of Xml.
Stability Index	The factor by which the flow energy requirement changes during repeat testing.
Flow Rate Index	The factor by which the flow energy requirement is changed when the flow rate is reduced by a factor of 10.
Specific Energy	The energy needed to displace a conditioned powder using a gentle shearing and lifting mode of displacement. This energy is then divided by the split mass
Conditioned Bulk Density	The bulk density of Xml of conditioned powder
Aerated Energy	The flow energy measured when air is being passed through the powder at a velocity of vmm/s.
Aeration Ratio	The factor by which the flowability energy is Reduced by aeration at an air velocity of vmm/s.
Aeration Sensitivity	The maximum rate of reduction of flow energy with respect to air velocity